# Delivery of Small Interfering RNA by Peptide-Targeted Mesoporous Silica Nanoparticle-Supported Lipid Bilayers

**Carlee E. Ashley,[†,⊥,*] Eric C. Carnes,[‡,⊥,§] Katharine E. Epler,[§] David P. Padilla,[§] Genevieve K. Phillips,[⊥] Robert E. Castillo,[§] Dan C. Wilkinson,[§] Brian S. Wilkinson,[§] Cameron A. Burgard,[§] Robin M. Kalinich,[‖] Jason L. Townson,[§] Bryce Chackerian,[⊥,△] Cheryl L. Willman,[⊥,#] David S. Peabody,[⊥,△] Walker Wharton,[⊥,#] and C. Jeffrey Brinker[‡,§,⊥,△,▽,*]**

[†]Biotechnology and Bioengineering Department, Sandia National Laboratories, Livermore, California 94551-0969, United States, [‡]Department of Chemical and Nuclear Engineering, University of New Mexico, Albuquerque, New Mexico 87131, United States, [§]Center for Micro-Engineered Materials, University of New Mexico, Albuquerque, New Mexico 87131, United States, [⊥]Cancer Research and Treatment Center, University of New Mexico Health Sciences Center, Albuquerque, New Mexico 87131, United States, [‖]Ceramic Processing and Inorganic Materials Department, Sandia National Laboratories, Albuquerque, New Mexico 87185-1349, United States, [#]Department of Pathology, University of New Mexico Health Sciences Center, Albuquerque, New Mexico 87131, United States, [△]Department of Molecular Genetics and Microbiology, University of New Mexico Health Sciences Center, Albuquerque, New Mexico 87131, United States, and [▽]Self-Assembled Materials Department, Sandia National Laboratories, Albuquerque, New Mexico 87185-1349, United States

**ABSTRACT** The therapeutic potential of small interfering RNAs (siRNAs) is severely limited by the availability of delivery platforms that protect siRNA from degradation, deliver it to the target cell with high specificity and efficiency, and promote its endosomal escape and cytosolic dispersion. Here we report that mesoporous silica nanoparticle-supported lipid bilayers (or "protocells") exhibit multiple properties that overcome many of the limitations of existing delivery platforms. Protocells have a 10- to 100-fold greater capacity for siRNA than corresponding lipid nanoparticles and are markedly more stable when incubated under physiological conditions. Protocells loaded with a cocktail of siRNAs bind to cells in a manner dependent on the presence of an appropriate targeting peptide and, through an endocytic pathway followed by endosomal disruption, promote delivery of the silencing nucleotides to the cytoplasm. The expression of each of the genes targeted by the siRNAs was shown to be repressed at the protein level, resulting in a potent induction of growth arrest and apoptosis. Incubation of control cells that lack expression of the antigen recognized by the targeting peptide with siRNA-loaded protocells induced neither repression of protein expression nor apoptosis, indicating the precise specificity of cytotoxic activity. In terms of loading capacity, targeting capabilities, and potency of action, protocells provide unique attributes as a delivery platform for therapeutic oligonucleotides.

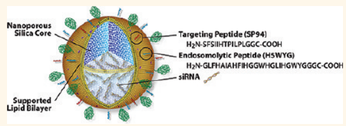


**KEYWORDS:** mesoporous silica nanoparticle · supported lipid bilayer · lipid nanoparticle · targeted delivery · peptide ligand · small interfering RNA · cancer

The delivery of cancer therapeutic agents sequestered in nanoparticles has the potential to bypass many severe problems associated with systemic drug administration.[1,2] Encapsulation allows treatment with compounds that are poorly soluble and/or unstable in physiological solutions, as well as those that are rapidly metabolized or cleared when administered as free drugs. Conjugation of the particle with a targeting moiety that recognizes an antigen overexpressed on the surface of a tumor cell results in a series of additional benefits, including mitigating damage to normal cells and a marked dose escalation that results from the localized release of highly concentrated drugs at the site of a tumor or within a cancer cell.[3] The therapeutic potential of many classes of macromolecules, especially nucleic acids and proteins, is severely limited because of degradation by plasma enzymes or an induction of an immune response following systemic administration. In addition, cellular uptake is typically restricted due to issues with either size or charge. The ability to package these molecules within particles overcomes such impediments and allows evaluation of the therapeutic efficacy of a large number of agents not presently available for clinical applications.

The discovery of RNA interference (RNAi) as a robust modulator of eukaryotic gene expression has provided unique insights into cellular pathways that regulate a number of fundamental biological processes.[4,5] In addition, it has allowed the development of a new class of reagents with powerful therapeutic potential.[6,7] Under physiological conditions, double-stranded RNAs are recognized by Dicer, a type III RNase, and digested into 21–23 base pair fragments. The resulting cleavage product binds to an RNA-induced silencing complex (RISC) where the sense strand

* Address correspondence to ceashle@sandia.gov or cjbrink@sandia.gov.

Received for review October 24, 2011 and accepted February 6, 2012.

**Published online February 06, 2012**
10.1021/nn204102q

(relative to an endogenous mRNA) is discarded. RISC loaded with single-stranded RNA binds corresponding mRNAs in the cytoplasm and mediates either a translational repression or an enzymatic cleavage depending on the nature of the base pairing. On the basis of remarkable progress in identifying critical aspects of this pathway, it has become possible to envision utilizing the features of RNAi to treat any of a variety of diseases whose pathology can be modulated by a decrease in the expression of a specific gene product.[8] Small interfering RNA (siRNA) is a double-stranded RNA sequence with perfect homology to a region of a cellular message that can be either ectopically introduced into cells or generated from a precursor RNA expressed from a transfected plasmid or transduced virus.[9] siRNAs enter the RISC pathway and mediate cleavage of the targeted message, providing a mechanism whereby, in theory, any cellular mRNA can be inactivated in a precise and controlled manner. siRNAs are especially attractive as anticancer therapies,[10,11] since profound changes in the behavior or survival of neoplastic cells are induced by decreases in the expression of activated oncogenes, cell cycle regulators, or pro-apoptotic genes. The expression of transcripts whose products are involved in the induction of drug resistance can also be targeted by siRNAs. The cytotoxic activity of siRNAs has been clearly demonstrated in a number of *in vitro* and *in vivo* model systems.[12] Davis *et al*. recently extended these studies by reporting that the systemic administration of siRNA encapsulated in targeted nanoparticles repressed gene expression in the tumor cells of human patients.[13] Therefore, targeted delivery of RNAi agents promises to enable effective treatment of a variety of cancers.

Despite this promise, however, it is clear that a number of significant barriers must be overcome before the widespread clinical use of siRNA technology becomes feasible. Several issues, including ensuring specificity for the target gene, prolonging the duration of siRNA activity, and preventing the induction of an innate immune response, have been addressed, at least to some extent, by a careful consideration of siRNA sequences and chemical modifications of the ribose backbone structure.[14−16] The major obstacle remaining for the development of successful siRNA therapeutics is an optimization of the multiple components of an efficient delivery system.[17,18] Localized delivery of RNAi constructs has been achieved in a number of animal models and is the basis of a series of clinical trials, predominately investigating intervention into pathologies of the eye.[19] Systemic applications will be required for the treatment of many diseases, including most tumors, where targeted cells are widely dispersed. In this case, it will be necessary for siRNAs to be administered in a form that protects them from degradation by plasma nucleases and that enables them to circulate for sufficient periods of time, deposit at sites of disease, selectively interact with target cells, and undergo internalization in such a way that they are released into the cytosol and enter the RISC pathway. Each of these steps represents a significant technical barrier, and, while some progress has been made in the development of appropriate delivery protocols, no single formulation has yet addressed all of these concerns.

We recently described a novel and remarkably versatile nanocarrier, the mesoporous silica nanoparticle-supported lipid bilayer, or "protocell'", which synergistically combines features of both mesoporus silica particles[20−30] and liposomes to exhibit many features of an ideal targeted therapeutic delivery platform;[31] we selected the term "protocell" to suggest that these particles, since they consist of a lipid bilayer supported on a spherical scaffold filled with biomolecular cargos, can be viewed as a reductionist cellular construct. As shown in Figure 1, protocells are formed *via* fusion of liposomes to porous silica nanoparticles. The high pore volume and surface area of the spherical mesoporous silica core allow high-capacity encapsulation of a spectrum of cargos. The supported lipid bilayer, whose composition can be modified for specific biological applications, serves as a modular, reconfigurable scaffold, allowing the attachment of a variety of molecules that provide cell-specific targeting and controlled intracellular trafficking. We have found that protocells loaded with low molecular weight therapeutic agents and conjugated with a peptide that specifically recognizes hepatocellular carcinomas induce cytotoxicity with a $10^6$-fold improvement in efficacy compared to corresponding liposomes.[31] Here we describe the ability of protocells to serve as a delivery platform for siRNAs. The unique characteristics of targeted protocells address many of the deficiencies that currently limit the clinical use of these macromolecular agents.

## RESULTS

**Synthesis and Characterization of siRNA-Loaded Protocells.** Mesoporous silica nanoparticles were prepared using the emulsion processing technique described by Carroll *et al*.[32] and were characterized by a Brunauer−Emmett−Teller surface area of 850 $m^2$/g, a pore volume fraction of ∼65%, and a multimodal pore morphology composed of large (23−30 nm), surface-accessible pores interconnected by 3−13 nm pores (see Figure 2A and D). Silica nanoparticles were size-separated before being loaded with siRNA as described in the Methods section, resulting in particles with an average diameter of 165 nm (see Figure 2B). PEGylated liposomes were then fused to siRNA-loaded cores, and the resulting supported lipid bilayer was chemically conjugated with a targeting peptide (SP94) and an endosomolytic peptide (H5WYG), the sequences of which are given in Figure 1.

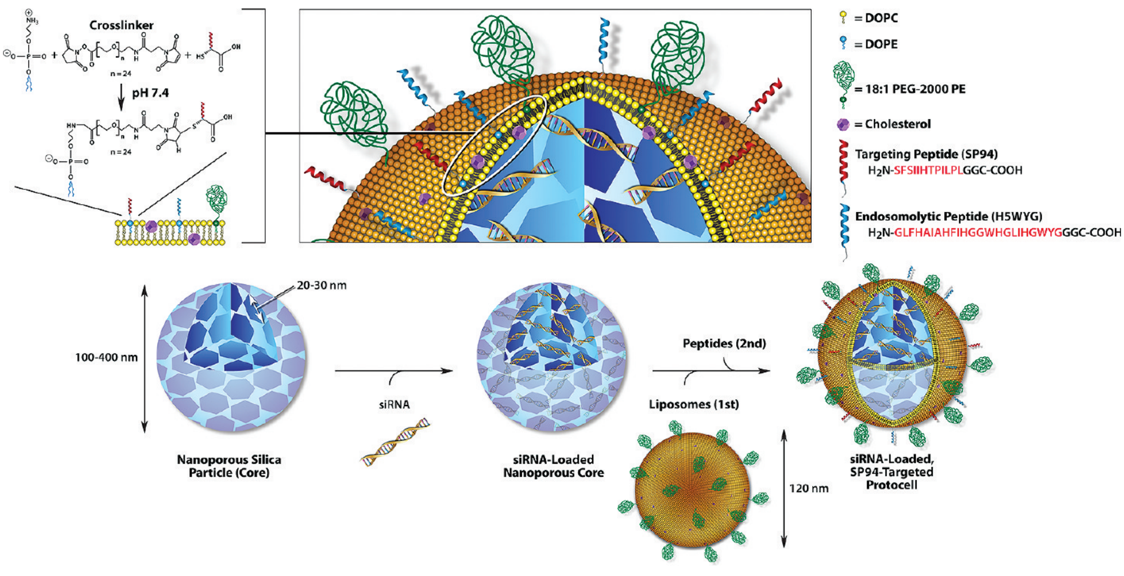


**Figure 1. Schematic depicting the process used to synthesize siRNA-loaded mesoporous silica nanoparticle-supported lipid bilayers (protocells). To form protocells loaded with therapeutic RNA and targeted to hepatocellular carcinomas (HCC), mesoporous silica cores modified with an amine-containing silane (AEPTMS) were first soaked in a solution of small interfering RNA (siRNA). Liposomes composed of DOPC, DOPE, cholesterol, and 18:1 PEG−2000 PE (55:5:30:10 mass ratio) were then fused to siRNA-loaded cores. The resulting supported lipid bilayer (SLB) was modified with a targeting peptide (SP94) that binds to HCC and an endosomolytic peptide (H5WYG) that promotes endosomal/lysosomal escape of internalized protocells. Peptides, modified with glycine−glycine (GG) spacers and C-terminal cysteine residues, were conjugated to primary amines present in DOPE moieties *via* a heterobifunctional cross-linker (SM(PEG)$_{24}$) with a 9.5 nm polyethylene glycol (PEG) spacer. The SP94 and H5WYG sequences reported by Lo *et al.*[61] and Moore *et al.*[62] are given in red.**

The siRNA loading capacity of protocells is compared to that of zwitterionic and cationic lipid nanoparticles (LNPs) in Figure 3A. Cationic lipids and polymers form the basis of most commercially available transfection reagents and nonviral siRNA delivery vehicles,[33] making LNPs, also referred to as lipoplexes and liposomes, the most appropriate system by which to judge the performance of protocells. LNPs composed of the zwitterionic phospholipid DOPC encapsulated ∼10 pmol of siRNA per $10^{10}$ particles. Construction of LNPs composed of the cationic lipid DOTAP resulted in a 5-fold increase in the siRNA cargo, presumably due to attractive electrostatic interactions between the negatively charged oligonucleotide and the positively charged lipid components. Protocells containing a negatively charged silica core with a zwitterionic (DOPC) lipid bilayer had a capacity roughly equivalent to the cationic LNP. Modification of the silica core with the amine-containing silane 3-[2-(2-aminoethylamino)ethylamino]propyltrimethoxysilane (AEPTMS) increased the zeta potential ($\zeta$) from −32 mV to +12 mV and resulted in a siRNA capacity of ∼1 nmol per $10^{10}$ particles. Use of DOTAP liposomes to synergistically load siRNA into negatively charged cores[34] resulted in protocells with a similar capacity, more than 100-fold higher than that of the zwitterionic LNPs that are commonly utilized in particle-based therapeutic applications. DOPC protocells with AEPTMS-modified cores were selected for further studies due to their high capacity for siRNA and their low intrinsic cytotoxicity (see Supplementary Figure 1). It should be noted that siRNA-loaded protocells were slightly larger (178 ± 24.3 nm) than siRNA-loaded DOPC LNPs (135 ± 19.1 nm) and DOTAP LNPs (144 ± 14.8 nm), resulting in a ∼2-fold increase in particle volume. When the capacities shown in Figure 3A are normalized against particle volume, however, DOPC protocells with AEPTMS-modified cores still encapsulate 50- and 10-fold more siRNA than DOPC and DOTAP LNPs, respectively, which demonstrates that the high-surface-area mesoporous silica core confers a higher intrinsic loading capacity than that expected based on volumetric differences alone. Furthermore, since the positively charged core promotes electrostatic-driven loading of siRNA, zwitterionic lipids can be used to form the protocell's supported lipid bilayer, thereby eliminating cytotoxicity associated with delivery vehicles that employ cationic lipids to complex siRNA (see Supplementary Figure 1).

Panels B and C of Figure 3 compare the siRNA release profiles of DOPC protocells with AEPTMS-modified cores with those of DOPC and DOTAP LNPs upon dispersion in either a surrogate biological fluid at pH 7.4 or a pH 5.0 buffer that mimics endosomal conditions. DOPC LNPs rapidly released their encapsulated siRNA under both neutral and mildly acidic pH conditions, resulting in a complete loss of the nucleotide content within 4−12 h. Although DOTAP LNPs were more stable than DOPC LNPs under neutral pH conditions, approximately 50% of their siRNA content was lost over a 72 h period. In marked contrast to both LNPs, DOPC protocells with AEPTMS-modified cores

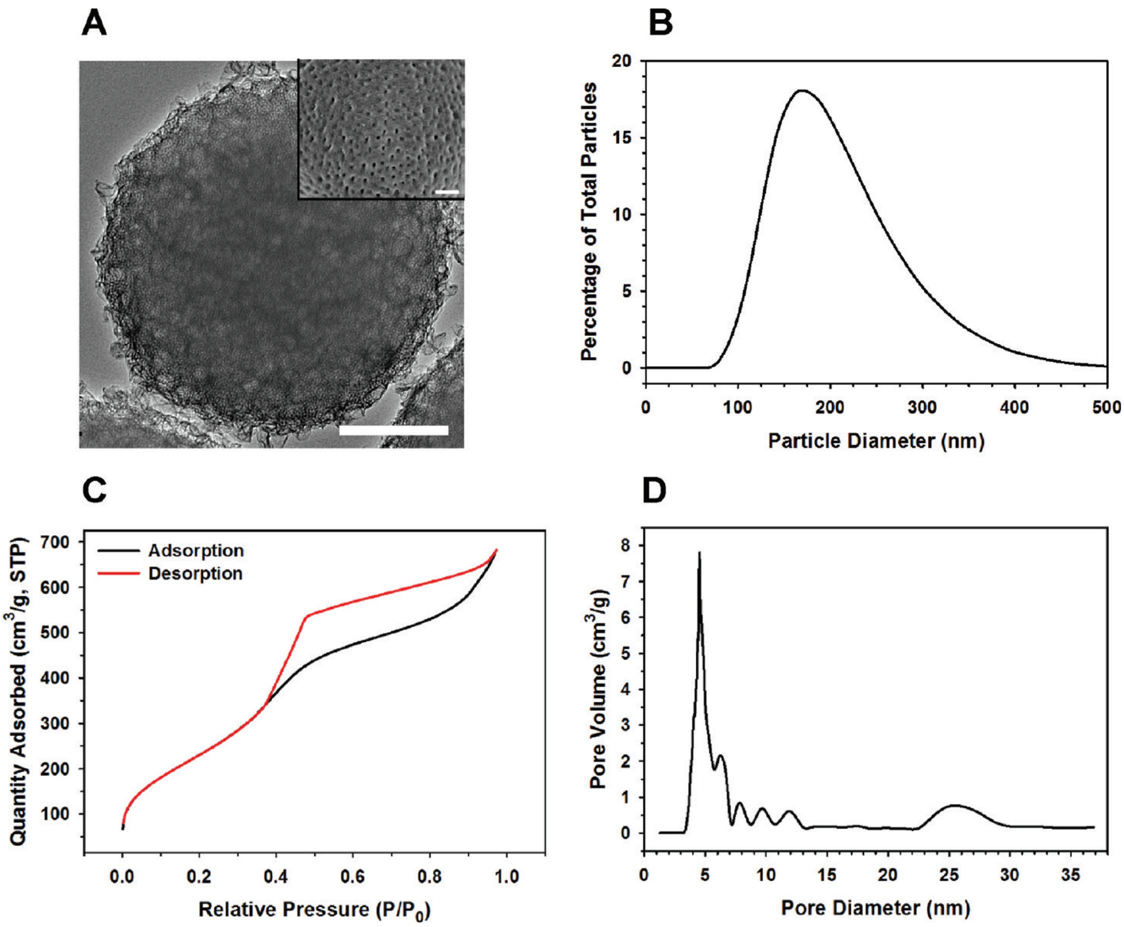


Figure 2. Characterization of the mesoporous silica nanoparticles that form the protocell core. (A) Transmission electron microscopy (TEM) image of multimodal silica nanoparticles formed *via* the emulsion processing technique described by Carroll *et al.*[32] Scale bar = 100 nm. The inset shows a scanning electron microscopy (SEM) image of a 5 $\mu$m multimodal silica particle, in which surface-accessible pores are visible; large particles were used to enhance resolution. Inset scale bar = 200 nm. (B) Dynamic light scattering (DLS) of multimodal silica nanoparticles after size-based separation. Resulting particles had an average diameter of ~165 nm. (C) Nitrogen sorption isotherm for size-separated multimodal silica nanoparticles. The presence of hysteresis is consistent with a network of larger pores interconnected by smaller pores. (D) A cumulative pore volume plot, calculated from the adsorption branch of the isotherm in (C) using the Barrett–Joyner–Halenda model, demonstrates the presence of large (23–30 nm) pores and small (3–13 nm) pores.

retained 95% of their encapsulated RNA when exposed to the simulated body fluid for 72 h. Under mildly acidic conditions comparable to those in the endosome/lysosome pathway, the reduced electrostatic and dipolar interactions between the siRNA-loaded, AEPTMS-modified core and the PE and PC headgroups of the supported lipid bilayer caused membrane destabilization and exposure of the core to the acidic medium (see the Supporting Information of ref 31 for more details). After membrane destabilization, the combined rates of cargo diffusion and core dissolution resulted in the release profile seen in Figure 3C. Thus, in terms of siRNA loading capacity, particle stability, and release characteristics, protocells represent a dramatic improvement over corresponding LNPs prepared using state-of-the-art techniques.

**Gene-Specific Silencing by siRNA-Loaded Protocells.** We recently demonstrated that protocells, when conjugated with a targeting peptide (SP94) that binds to hepatocellular carcinomas (HCC) but not control hepatocytes, can deliver a wide variety of chemotherapeutic agents and selectively induce apoptosis in tumor cells that express the relevant surface antigen.[31] Here we markedly expand the characterization of SP94-targeted protocells loaded with siRNA. We prepared protocells composed of AEPTMS-modified silica cores and a DOPC/DOPE/cholesterol/PEG-2000 (55:5:30:10 mass ratio) supported lipid bilayer conjugated with both SP94, to confer selective binding to HCC, and an endosomolytic peptide (H5WYG), to promote endosomal/lysosomal escape. Protocells were loaded with an equimolar mixture of siRNAs that target members of the cyclin superfamily, including cyclin A2, cyclin B1, cyclin D1, and cyclin E, proteins intimately involved in the regulation of both cell cycle traverse and cell viability.[35]

The concentration and time dependence of gene silencing in the HCC line Hep3B by siRNA-loaded, SP94-targeted DOPC protocells constructed with

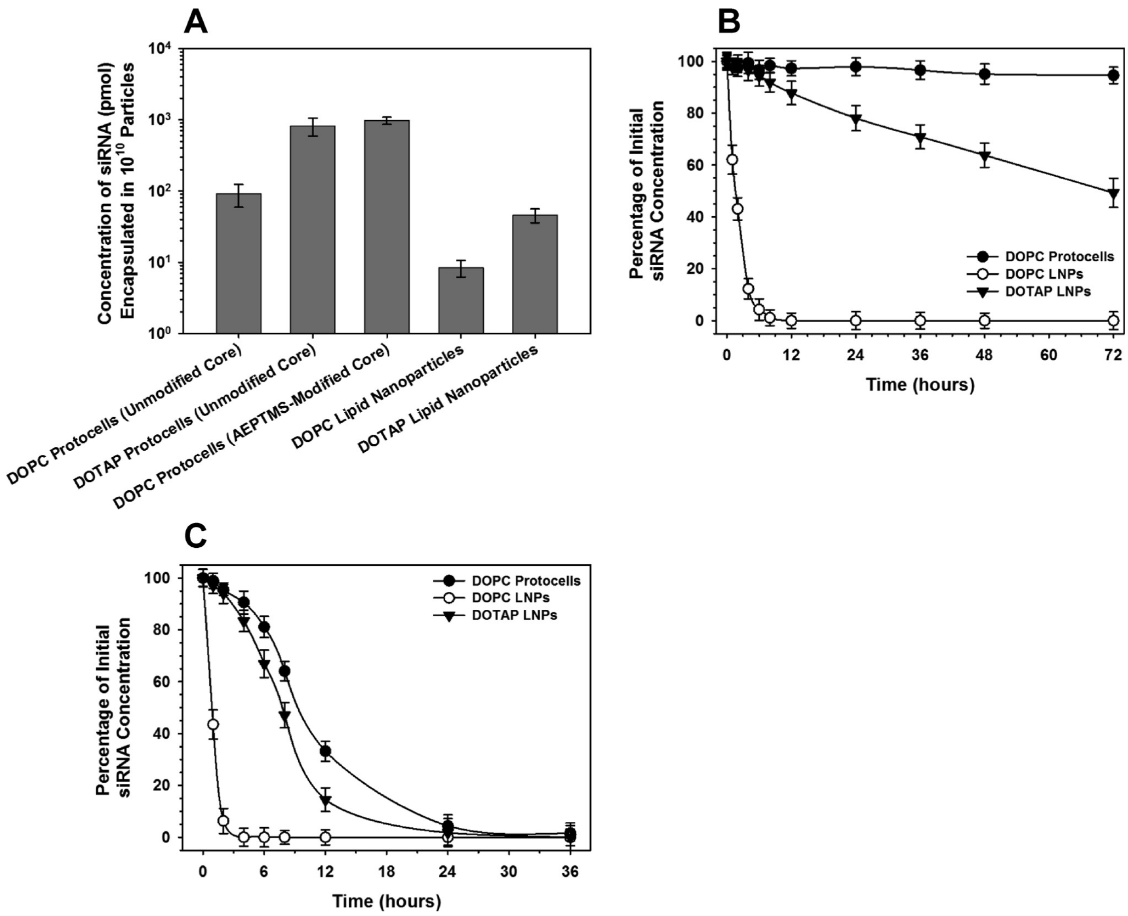


**Figure 3. Protocells have a high capacity for siRNA, the release of which is triggered by acidic pH. (A) Concentrations of siRNA that can be loaded within $10^{10}$ protocells and lipid nanoparticles (LNPs). Zeta potential values for unmodified and AEPTMS-modified silica cores in 0.5× PBS (pH 7.4) are −32 and +12 mV, respectively. (B and C) Rates at which siRNA is released from DOPC protocells with AEPTMS-modified cores, DOPC LNPs, and DOTAP LNPs upon exposure to a pH 7.4 simulated body fluid (B) or a pH 5.0 buffer (C) at 37 °C. The average diameters of siRNA-loaded protocells, DOPC LNPs, and DOTAP LNPs were 178 nm (±24.3 nm), 135 nm (±19.1 nm), and 144 nm (±14.8 nm), respectively. Error bars represent 95% confidence intervals (1.96 $\sigma$) for $n$ = 3.**

AEPTMS-modified cores are shown in Figure 4. Panel A demonstrates that increasing concentrations of protocells and, thereby, increasing concentrations of siRNA induced a dose-dependent decrease in the protein levels of each of the targeted genes within 48 h. The concentrations of siRNA required to repress protein expression by 90% ($IC_{90}$) were 125.3, 92.1, 149.0, and 370.4 pM for cyclin A2, cyclin B1, cyclin D1, and cyclin E, respectively. Panel B shows how protein levels decreased upon addition of 125 pM of siRNA loaded within targeted protocells. By 72 h, the level of each of the targeted proteins was repressed by nearly 90%, with the degree of repression reflecting the differences in $IC_{90}$ values. Cyclin A2 mRNA levels, as determined by real-time PCR, are included in Figure 4A and B to provide further evidence that RNAi was responsible for the dose- and time-dependent decreases in cyclin protein concentrations. Corresponding data for free cyclin-specific siRNA, DOTAP LNPs loaded with cyclin-specific siRNA, and SP94-targeted protocells loaded with Silencer Select negative control siRNA are included in the Supporting Information (see Supplementary Figures 2 and 3); $IC_{90}$ values for DOTAP LNPs loaded with cyclin A2, cyclin B2, cyclin D1, or cyclin E-specific siRNA were 331.5, 223.9, 543.6, and 1883.7 pM, respectively (see Supplementary Table 1).

Figure 4C shows the selectivity of gene silencing achievable with various types of SP94-targeted particles. DOPC protocells loaded with 125 pM siRNA induced nearly complete repression of cyclin A2 protein expression following 48 h of incubation with Hep3B but had no effect on nontransformed hepatocytes. In contrast, SP94-targeted DOTAP LNPs loaded with 125 pM siRNA induced a ~60% repression of cyclin A2 expression in Hep3B but also decreased cyclin A2 levels in hepatocytes, an effect likely due to nonspecific uptake mediated by their positive charge ($\zeta$ = +22 mV in 0.5× PBS, versus $\zeta$ = −3.3 mV for PEGylated DOPC protocells). The numbers of SP94-targeted DOPC protocells and DOTAP LNPs required to repress cyclin A2 expression by 90% is shown on the right axis in panel C; 300-fold fewer DOPC protocells were required than DOTAP LNPs. Thus, in terms of both

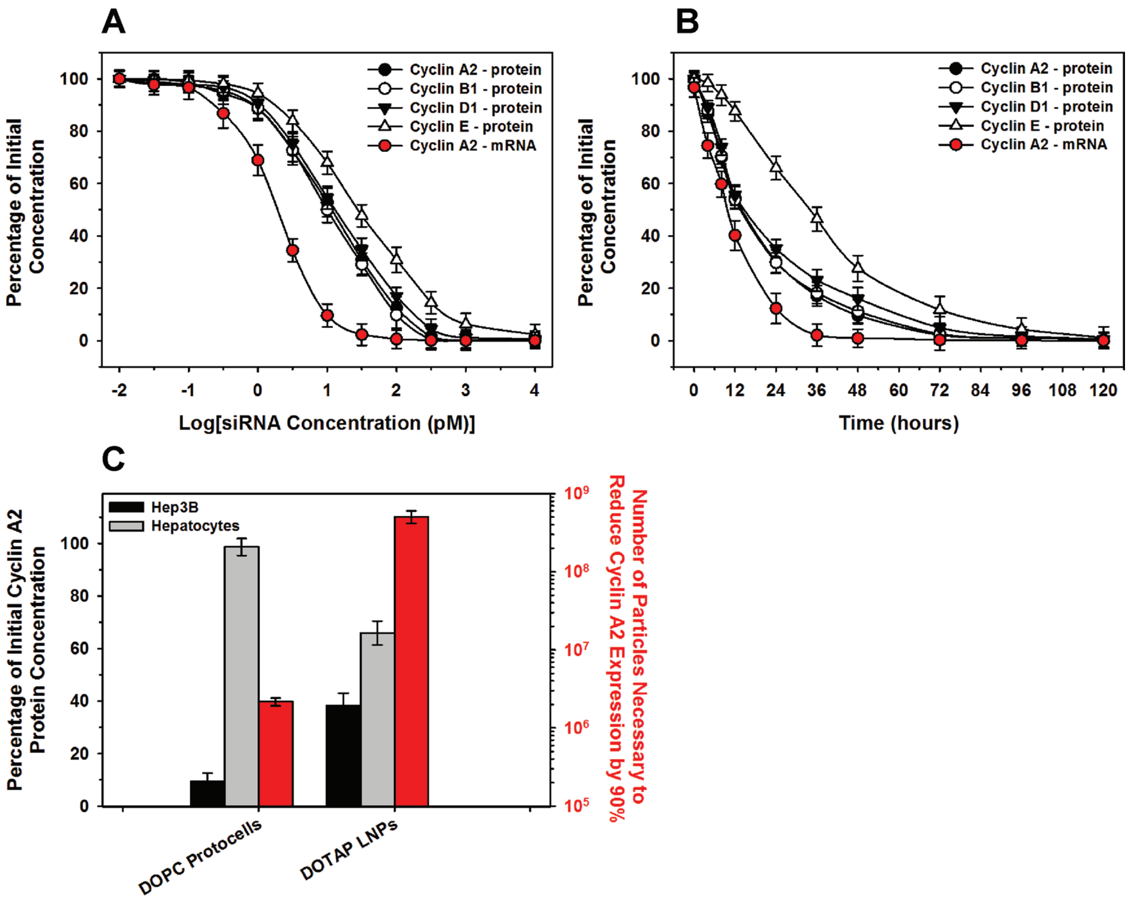


Figure 4. siRNA-loaded, SP94-targeted protocells silence various cyclin family members in HCC but not hepatocytes. Dose-(A) and time (B)-dependent decreases in the expression of cyclin A2, B1, D1, and E protein upon exposure of Hep3B to siRNA-loaded, SP94-targeted protocells. $1 \times 10^6$ cells were continually exposed to various concentrations of siRNA for 48 h in (A) and to 125 pM siRNA for various periods of time in (B). Cyclin A2 mRNA levels are included for comparison. Protein concentrations were determined *via* flow cytometry analysis of cells stained by immunofluorescence. mRNA concentrations were determined by real-time PCR. (C, left axis) Percentages of initial cyclin A2 protein concentrations that remain upon exposure of $1 \times 10^6$ Hep3B or hepatocytes to 125 pM siRNA, loaded within DOPC protocells or DOTAP lipid nanoparticles (LNPs), for 48 h at 37 °C. (C, right axis) The number of siRNA-loaded, SP94-targeted DOPC protocells or DOTAP LNPs that must be incubated with $1 \times 10^6$ Hep3B cells to reduce expression of cyclin A2 protein to 10% of the initial concentration. DOPC LNPs were omitted from these experiments, as well as all subsequent analyses, as their efficacy was similar to that of free siRNA. Protocell SLBs were composed of DOPC with 5 wt % DOPE, 30 wt % cholesterol, and 10 wt % PEG-2000 and were modified with 0.015 wt % SP94 and 0.500 wt % H5WYG. DOTAP LNPs were prepared using a 55:5:30:10 ratio of DOTAP:DOPE:cholesterol:PEG-2000 PE and were modified with 0.015 wt % SP94 and 0.500 wt % H5WYG. Error bars represent 95% confidence intervals (1.96 $\sigma$) for $n = 3$.

activity and specificity, targeted protocells offer marked advantages over lipid-based nanoparticles.

Representative confocal fluorescence microscopy images illustrating the time dependence of cyclin A2, B1, D1, and E expression in cells exposed to siRNA-loaded, SP94-targeted protocells are shown in Figure 5. As demonstrated in panel A, 1 h after addition of protocells to Hep3B, the expression of each of the proteins remained at control levels, and the silica cores were present in a punctuate pattern, suggesting endosomal localization (see ref 31 for details about the internalization pathway of SP94-targeted protocells). By 48 h, silica was distributed throughout the Hep3B cells, which were likely in the late stages of apoptosis, as indicated by their rounded morphologies and fragmented nuclei, and the expression of each of the targeted proteins was repressed to background levels. In comparison, an identical treatment of nontransformed hepatocytes resulted in neither the cellular accumulation of protocells nor the repression of protein expression (see panel B).

**Induction of Growth Arrest and Apoptosis by siRNA-Loaded Protocells.** The ability of siRNA-loaded, SP94-targeted protocells to selectively induce growth arrest and apoptosis of HCC is demonstrated by Figure 6. Panel A shows that protocells loaded with 125 pM of the siRNA cocktail resulted in decreased proliferation of Hep3B, as determined by decreased incorporation of 5-bromo-2′-deoxyuridine (BrdU), an assay widely used to quantify newly synthesized DNA in actively proliferating cells. Additionally, as demonstrated in panel B, siRNA-loaded protocells caused Hep3B cells to accumulate in $G_1/G_0$ and $G_2/M$, an effect most clearly indicated by the decrease in S phase cells. The $G_1$

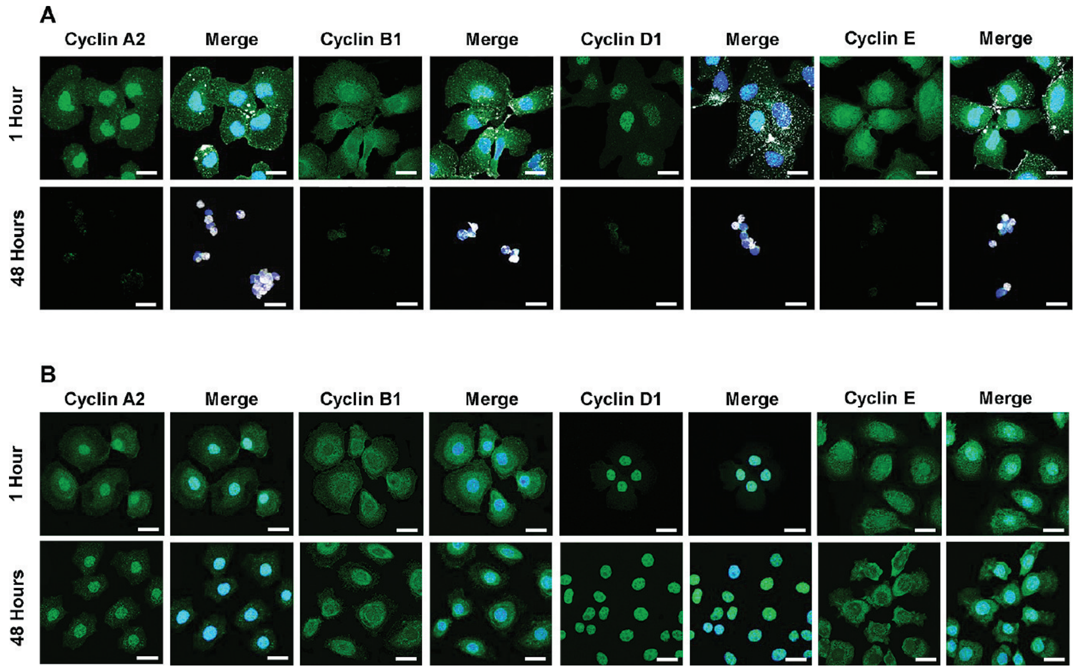


**Figure 5. Confocal fluorescence microscopy images of Hep3B (A) and hepatocytes (B) after exposure to siRNA-loaded, SP94-targeted protocells for 1 or 48 h at 37 °C. Cells were incubated with a 10-fold excess of Alexa Fluor 647-labeled protocells (white) prior to being fixed, permeablized, and stained with Hoechst 33342 (blue) and Alexa Fluor 488-labeled antibodies against cyclin A2, cyclin B1, cyclin D1, or cyclin E (green). Protocell SLBs were composed of DOPC with 5 wt % DOPE, 30 wt % cholesterol, and 10 wt % PEG-2000 and were modified with 0.015 wt % SP94 and 0.500 wt % H5WYG. Scale bars = 20 $\mu$m.**

arrest was caused by either a repression of cyclin D1, the activity of which is required for early $G_1$ transverse, or a loss of cyclins A2 and E, which mediate exit of cells from $G_1$ into S phase. The $G_2$ arrest was caused by a repression of cyclin B1, whose activity regulates entry of cells into mitosis.

Growth arrest was rapidly succeeded by apoptosis, as shown in panel C. Cells in the early stages of apoptosis were identified by an increase in annexin V binding, while cells in the late stages of apoptosis were identified by both annexin V and propidium iodide staining. A selective increase in the number of apoptotic Hep3B was observed as early as 12 h after addition of siRNA-loaded, SP94-targeted protocells, and over 90% of cells were positive for both apoptosis markers by 72 h, which corresponds to the time required for cyclin levels to fall to $\leq$10% of their original values and for ~90% of cells to become arrested in $G_0/G_1$ or $G_2$/M. In contrast, no cytotoxicity was observed in nontransformed hepatocytes, which is confirmed by the representative microscopy images shown in Figure 7. Panel A demonstrates that the entire population of Hep3B became positive for surface-bound annexin V and nuclear-bound propidium iodide within 48 h, while panel B shows that control hepatocytes remained negative for both markers of apoptosis. The left axis of Figure 6D compares the percentage of Hep3B and hepatocytes that became positive for annexin V and propidium iodide staining upon exposure to DOPC protocells or DOTAP LNPs, both loaded with 125 pM of the cyclin-specific siRNA cocktail, while the right axis plots the number of siRNA-loaded, SP94-targeted DOPC protocells and DOTAP LNPs that were necessary to induce apoptosis in 90% of Hep3B. This panel demonstrates that protocells effectively induced apoptosis in Hep3B at a particle:cell ratio of ~10 (*i.e.*, ~1 $\times$ $10^7$ protocells per 1 $\times$ $10^6$ cells) without affecting the viability of control hepatocytes. In comparison, 200-fold more DOTAP LNPs were required to kill 90% of the Hep3B population, and, at a siRNA concentration of 125 pM, DOTAP LNPs caused a ~30% reduction in hepatocyte viability, an effect that was even more dramatic at the particle concentration necessary to induce apoptosis in the majority of Hep3B.

## DISCUSSION

The full potential of therapeutic RNAs, which are under extensive investigation for the treatment of many diseases mediated by aberrant patterns of gene expression, remains unfulfilled due to marked deficiencies in delivery systems.[17,18] In this paper, we present evidence indicating that protocells exhibit characteristics that enable efficient encapsulation and cell-specific delivery of siRNAs.

Unmodified nucleic acids, including siRNA, cannot be systemically administered for several reasons. They are highly susceptible to plasma nucleases and have a very short circulation half-life due to efficient renal filtration.[3] In addition, nucleic acids are not readily taken up by cells because of their net negative charge

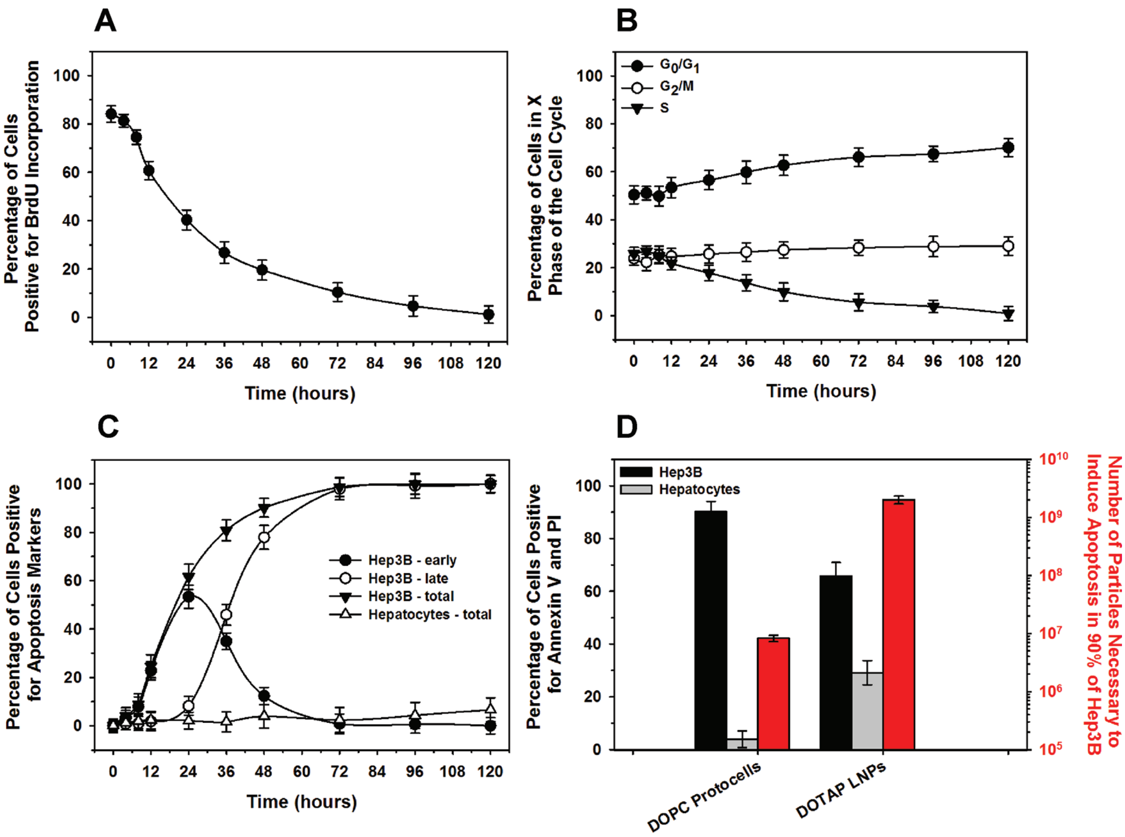


**Figure 6. SP94-targeted protocells loaded with the cyclin-specific siRNA cocktail induce growth arrest and apoptosis in HCC without affecting hepatocyte viability. (A–C) The percentage of $1 \times 10^6$ Hep3B that were proliferating (A), arrested in $G_0/G_1$ or $G_2/M$ (B), or apoptotic (C) upon exposure to SP94-targeted protocells loaded with 125 pM of the cyclin-specific siRNA cocktail for various periods of time at 37 °C. Proliferation was determined using a flow cytometric assay for 5-bromo-2′-deoxyuridine (BrdU) incorporation, where cells positive for BrdU incorporation were considered to be actively proliferating. The numbers of cells in $G_0/G_1$, S, or $G_2/M$ phases of the cell cycle were determined *via* Hoechst 33342 staining followed by flow cytometry-based cell cycle analysis. Apoptosis was quantified using Alexa Fluor 488-labeled annexin V and propidium iodide (PI). Cells positive for annexin V were considered to be in the early stages of apoptosis, while cells positive for both annexin V and PI were considered to be in the late stages of apoptosis; the total number of apoptotic cells was determined by adding the numbers of cells in early and late apoptosis. (D, left axis) Percentages of $1 \times 10^6$ Hep3B or heaptocytes that become apoptotic, *i.e.*, double-positive for Alexa Fluor 488-labeled annexin V and PI, upon exposure to 125 pM of the siRNA cocktail, loaded within DOPC protocells or DOTAP lipid nanoparticles (LNPs), for 48 h at 37 °C. (D, right axis) Number of siRNA-loaded, SP94-targeted DOPC protocells or DOTAP LNPs that must be incubated with $1 \times 10^6$ Hep3B to induce apoptosis in 90% of cells in the population. Protocell SLBs were composed of DOPC with 5 wt % DOPE, 30 wt % cholesterol, and 10 wt % PEG-2000 and were modified with 0.015 wt % SP94 and 0.500 wt % H5WYG. DOTAP LNPs were prepared using a 55:5:30:10 ratio of DOTAP:DOPE:cholesterol:PEG-2000 PE and were modified with 0.015 wt % SP94 and 0.500 wt % H5WYG. Error bars represent 95% confidence intervals (1.96 $\sigma$) for $n = 3$.**

and large size.[36] To circumvent these issues, siRNAs have been conjugated to a variety of polymers or encapsulated in nanoparticles such as liposomes. siRNAs incorporated into neutral liposomes or conjugated to cationic lipids have increased stability and circulating half-life and, in the case of cationic complexes, enhanced electrostatically mediated delivery to cells.[37,38] Natural products, including chitosan[39] and cyclodextran,[40] have been used to form biologically active complexes with siRNAs. Conjugation with cationic polymers, such as polyethyleneimine, has also been shown to enhance the therapeutic efficiency of siRNA by helping to prevent degradation and enhance delivery.[41]

The therapeutic use of systemically administered siRNA requires delivery to specific organs or subsets of cells to enhance efficacy and decrease nonspecific toxicity. This is especially true in the case of anticancer therapies, where it is necessary to protect normal cells from the actions of cytotoxic siRNAs. Complications also arise if targeted cells exist at multiple locations in the body, as is the case with hematological tumors or metastatic disease, where neoplastic cells are widely disseminated. To address this issue, molecules that recognize antigens differentially expressed on the surfaces of targeted cells have been conjugated either directly to siRNAs or to particles that encapsulate the nucleotides. Receptor ligands, such as folate,[42] cholesterol,[43] and transferrin,[13] have been successfully used to direct the binding of siRNA complexes to cells that overexpress the respective cellular receptor. Antibodies that recognize appropriate molecules on target cells have also been used to direct selective binding of

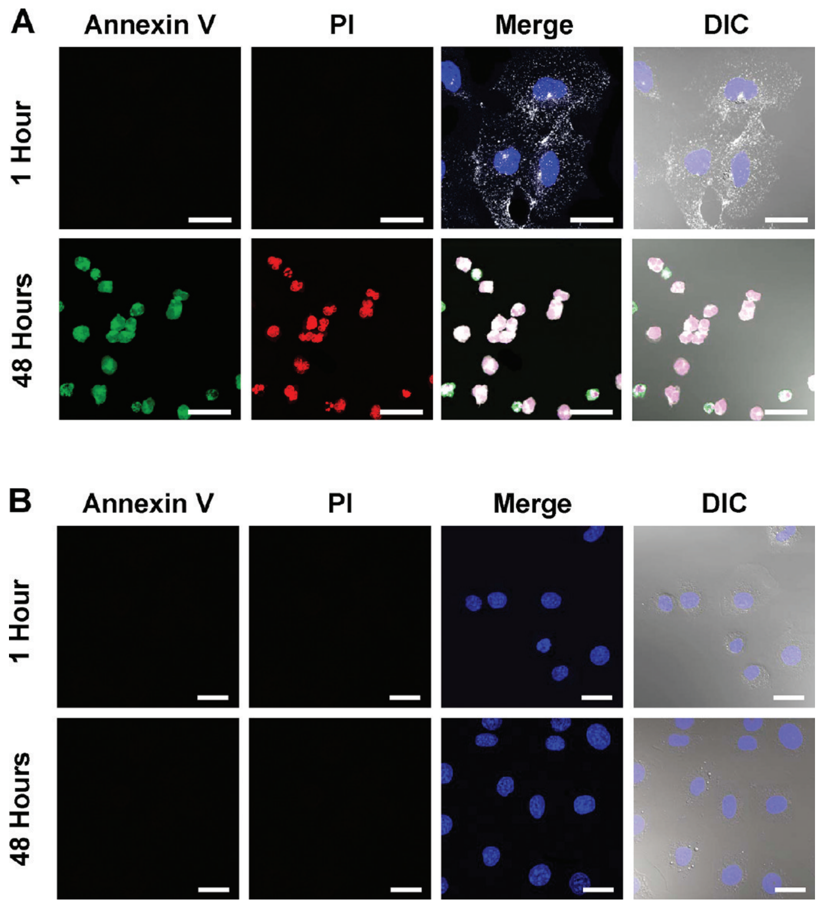


**Figure 7. Confocal fluorescence microscopy images of Hep3B (A) and hepatocytes (B) after exposure to siRNA-loaded, SP94-targeted protocells for 1 or 48 h at 37 °C. Cells were incubated with a 10-fold excess of Alexa Fluor 647-labeled protocells (white) prior to being stained with Hoechst 33342 (blue), Alexa Fluor 488-labeled annexin V (green), and propidium iodide (red). Differential interference contrast (DIC) images are included to show cell morphology. Protocell SLBs were composed of DOPC with 5 wt % DOPE, 30 wt % cholesterol, and 10 wt % PEG-2000 and were modified with 0.015 wt % SP94 and 0.500 wt % H5WYG. Scale bars = 20 $\mu$m.**

particles containing siRNAs to specific classes of cells.[44] Additionally, peptides or nucleic acid aptamers, selected by a multiplex screening procedure to bind desired cellular epitopes, have been conjugated directly to siRNAs or to classes of siRNA-containing particles to enhance specific cellular interactions.[45]

Despite the marked advances in some aspects of nucleic acid delivery systems, including modification of their chemical structure to protect against degradation or conjugation to targeting reagents, a number of deficiencies remain. While a number of reagents that employ cationic lipids or polymers to electrostatically complex, condense, and deliver nucleic acids are commercially available, the majority of these formulations result in the nonspecific transfection of eukaryotic cells. In addition, cationic lipid/nucleic acid complexes (lipid nanoparticles) have been found to be cytotoxic,[46] and their transfection efficiency and colloidal stability tend to be limited in the presence of serum. Conversely, zwitterionic lipids have a limited ability to efficiently compact nucleic acids, even in the presence of divalent cations. All such nanoparticle delivery systems also suffer from limited cargo capacities.

As shown by our experimental results, protocells offer significant advantages over existing delivery strategies. We have previously described their utility as targeted nanocarriers for small-molecule therapeutic agents and demonstrated that their cargo capacity, stability, and cell-specific cytotoxicity exceed those of traditional liposomes. Nanoparticle-based delivery of macromolecules presents even greater challenges due to their large size, charge characteristics, and potential issues with intracellular cargo release. Here we have shown that protocells offer distinct advantages in these applications as well. Multimodal porous silica nanoparticles can be rapidly loaded with nucleic acids, toxins, and macromolecular cocktails by soaking them in solutions of the desired cargo(s).[31] Fusion of DOPC liposomes to cargo-loaded cores results in the formation of a stabilized supported lipid bilayer that retains cargo at neutral pH, reduces nonspecific binding, improves colloidal stability, and mitigates the cytotoxicity associated with cationic liposomes and lipid nanoparticles (see ref 31 for more details). Targeting peptides conjugated to the fluid but stable SLB interact multivalently with cell surface receptors, inducing receptor-mediated endocytosis. Within the acidified endosomal environment, SLB destabilization, along with osmotic swelling and disruption of endosomes (caused by the proton sponge effect of endosomolytic peptides), results in dispersion of silica cores within the cytoplasm. Combined diffusion and silica core dissolution enable controlled, sustained cargo release for >12 h (see ref 31 for more details about successive steps of binding, endocytosis, and cytosolic dispersion of cargo). The combined capacity, stability, and targeting and internalization efficiency of protocells result in exceptionally low $IC_{90}$ values for Hep3B with practically no adverse effects on normal hepatocytes.

Protocells with 165 nm cores encapsulate, on average, $\sim 6 \times 10^4$ siRNA molecules per particle (per L) and retain nearly 100% of their cargo upon exposure to a simulated body fluid for 72 h. In comparison, lipid and polymer nanoparticles have a 10- to 1000-fold lower capacity for siRNA and are substantially less stable at neutral pH.[47,48] Protocells, furthermore, have a higher capacity for nucleic acid cargos than other mesoporous silica particles. S1MPs, developed by Tanaka *et al*. for sustained delivery of siRNA-loaded nanoliposomes to ovarian cancer, encapsulate approximately the same amount of RNA as protocells when volumetric differences are taken into account.[49] Polyethyleneimine-coated mesoporous silica nanoparticles, developed by Xia *et al*., complex $\sim 1$ $\mu$g of siRNA per 10 $\mu$g of particles (10 wt %);[30] in comparison, 10 $\mu$g of protocells can be loaded with $\sim 6.5$ $\mu$g of siRNA (65 wt %). Enhancements in capacity and stability enable siRNA-loaded protocells to silence target genes and induce apoptosis of HCC at concentrations that are 10 to 10 000 times less than values reported in the literature.[47,48,50−54] siRNA-loaded, SP94-targeted protocells silence 90% of cyclin A2, B1, D1, and E expression at siRNA concentrations ranging from 90 pM to 370 pM ($IC_{90}$) and kill >90% of HCC within 48 h at a siRNA concentration of 125 pM ($LC_{90}$). In comparison, targeted liposomes reported in the literature have $IC_{90}$ and $LC_{90}$ values of 5−500 nM, depending on the type of particle and conditions under which experiments were conducted.[50−52,54−56] The therapeutic efficacy of siRNA-loaded, SP94-targeted protocells exceeds that of polymer-encased mesoporous nanoparticles as well. Several groups have used mesoporous silica nanoparticles encapsulated within polycationic polymers to complex siRNA; such particles result in 30−60% knockdown of reporter and endogenous gene expression within 24−48 h at nanoparticle:siRNA (w/w) ratios of 10−20.[30,57] Since we load siRNA within the pores of AEPTMS-modified silica nanoparticles, the capacity of protocells is significantly higher, resulting in complete silencing of cyclin A2, B1, D1, and E expression at a protocell:cell ratio of $\sim 8$ (*i.e.*, $\sim 8 \times 10^6$ protocells per $1 \times 10^6$ cells). In conclusion, our findings suggest that protocells might serve as universal targeted nanocarriers for multiple classes of macromolecules, including siRNA. The mesoporous cores can also be loaded with other disparate cargo types, including the imaging and diagnostic agents needed for the burgeoning fields of theranostics and personalized medicine.

## MATERIALS AND METHODS

**Materials.** Antibodies against cyclin A2 (mouse mAb), cyclin B1 (mouse mAb), cyclin D1 (mouse mAb), and cyclin E (mouse mAb) were purchased from Abcam, Inc. (Cambridge, MA, USA). Silencer Select siRNAs (siRNA IDs for cyclins A2, B1, D1, and E are s2513, s2515, s229, and s2526, respectively), Silencer Select negative control siRNA, and the TaqMan Fast Cells-to-CT kit were purchased from Applied Biosystems by Life Technologies Corporation (Carlsbad, CA, USA). Human Hep3B (HB-8064), human hepatocytes (CRL-11233), Eagle's minimum essential medium (EMEM), Dulbecco's modified Eagle's medium (DMEM), fetal bovine serum (FBS), and 1× trypsin-EDTA solution (0.25% trypsin with 0.53 mM EDTA) were purchased from American Type Culture Collection (ATCC; Manassas, VA, USA). 1,2-Dioleoyl-*sn*-glycero-3-phosphocholine (DOPC), 1,2-dioleoyl-*sn*-glycero-3-phosphoethanolamine (DOPE), 1,2-dioleoyl-*sn*-glycero-3-phosphoethanolamine-*N*-[methoxy(polyethylene glycol)-2000] (18:1 PEG−2000 PE), 1,2-dioleoyl-3-trimethylammoniumpropane (DOTAP), and cholesterol were purchased from Avanti Polar Lipids, Inc. (Alabaster, AL, USA). ABIL EM 90 (cetyl PEG/PPG-10/1 dimethicone) was purchased from Evonik Industries (Essen, Germany). Hoechst 33342 (350/461), Alexa Fluor 488 antibody labeling kit (495/519), Alexa Fluor 488 conjugate of annexin V (495/519), Alexa Fluor 488-labeled mouse monoclonal antibody to BrdU (clone MoBU-1) (494/519), propidium iodide (535/617), Alexa Fluor 647 carboxylic acid succinimidyl ester (650/668), SlowFade Gold antifade reagent, Image-iT FX signal enhancer, 1× Dulbecco's phosphate-buffered saline (D-PBS), bovine albumin fraction V solution (BSA, 7.5%), and Lipofectamine RNAiMAX were purchased from Invitrogen Life Sciences (Carlsbad, CA, USA). BEGM bullet kits were purchased from Lonza Group Limited (Clonetics; Walkersville, MD, USA). Amicon Ultra-4 centrifugal filter units (10 kDa MWCO) were purchased from Millipore (Billerica, MA, USA). All peptides were synthesized by New England Peptide (Gardner, MA, USA). Succinimidyl-[(*N*-maleimidopropionamido)-tetracosaethylene glycol] ester ($SM(PEG)_{24}$) was purchased from Pierce Protein Research Products (Thermo Fisher Scientific LSR; Rockford, IL, USA). Ultrapure, EM-grade formaldehyde (16%, methanol-free) was purchased from Polysciences, Inc. (Warrington, PA, USA). Absolute ethanol, hydrochloric acid (37%), tetraethyl orthosilicate (TEOS, 98%), 3-[2-(2-aminoethylamino)ethylamino]propyltrimethoxysilane (AEPTMS, technical grade), hexadecyltrimethylammonium bromide (CTAB, ≥99%), sodium dodecyl sulfate (SDS, ≥98.5%), Triton X-100, hexadecane (≥99%), *tert*-butanol (≥99.5%), 2-mercaptoethanol (≥99.0%), DL-dithiothreitol (≥99.5%), dimethyl sulfoxide (≥99.9%), pH 5 citric acid buffer, ethylenediaminetetraacetic acid (EDTA, 99.995%), sodium tetraborate (99%), glycine (≥99%), 5-bromo-2′-deoxyuridine (BrdU, ≥ 99%), goat serum, human epidermal growth factor, L-α-phosphatidylethanolamine, bovine fibronectin, bovine collagen type I, soybean trypsin inhibitor (≥98%), DMEM without phenol red, and Sephadex G-200 were purchased from Sigma-Aldrich (St. Louis, MO, USA). Holey carbon-coated copper TEM grids were purchased from SPI Supplies (West Chester, PA, USA).

**Cell Culture Conditions.** Hep3B and hepatocytes were obtained from ATCC and grown per the manufacturer's instructions. Briefly, Hep3B was maintained in EMEM with 10% FBS. Hepatocytes were grown in flasks coated with BSA, fibronectin, and bovine collagen type I; the culture medium used was BEGM (gentamycin, amphotericin, and epinephrine were discarded from the BEGM bullet kit) with 5 ng/mL epidermal growth factor, 70 ng/mL phosphatidylethanolamine, and 10% FBS. Cells were maintained at 37 °C in a humidified atmosphere (air supplemented with 5% $CO_2$) and passaged with 0.05% trypsin at a subcultivation ratio of 1:3.

**Synthesis of Multimodal Silica Nanoparticles.** The emulsion processing technique used to synthesize mesoporous silica nanoparticles with multimodal porosity has been described by Carroll *et al*.[32] Briefly, 1.82 g of CTAB (soluble in the aqueous phase) was added to 20 g of deionized water, stirred at 40 °C until dissolved, and allowed to cool to 25 °C. Then 0.57 g of 1.0 N HCl, 5.2 g of TEOS, and 0.22 g of NaCl were added to the CTAB solution, and the resulting sol was stirred for 1 h. An oil phase composed of hexadecane with 3 wt % ABIL EM 90 (a nonionic emulsifier soluble in the oil phase) was prepared. The precursor sol was combined with the oil phase (1:3 volumetric ratio of sol: oil) in a 1000 mL round-bottom flask, stirred vigorously for 2 min to promote formation of a water-in-oil emulsion, affixed to a rotary evaporator (R-205; Buchi Laboratory Equipment; Switzerland), and placed in an 80 °C water bath for 30 min. The mixture was then boiled under a reduced pressure of 120 mbar (35 rpm for 3 h) to remove the solvent. Particles were then centrifuged (model Centra MP4R; International Equipment Company; Chattanooga, TN, USA) at 3000 rpm for 20 min, and the supernatant was decanted. Finally, the particles were calcined at 500 °C for 5 h to remove surfactants and other excess organic matter.

To make unmodified particles more hydrophilic, they were treated with (i) 4% (v/v) ammonium hydroxide and 4% (v/v) hydrogen peroxide and (ii) 0.4 M HCl and 4% (v/v) hydrogen peroxide for 15 min at 80 °C. Particles were then washed several times with water and resuspended in 0.5× D-PBS at a final concentration of 25 mg/mL. Mesoporous cores were modified with the amine-containing silane AEPTMS by adding 25 mg of calcined particles to 1 mL of 20% AEPTMS in absolute ethanol; the particles were incubated in AEPTMS for 4−6 h at room temperature, centrifuged (5000 rpm, 1 min) to remove unreacted AEPTMS, and resuspended in 1 mL of 0.5× D-PBS. AEPTMS-modified particles were fluorescently labeled by adding 5 $\mu$L of an amine-reactive fluorophore (Alexa Fluor 647 carboxylic acid, succinimidyl ester; 1 mg/mL in DMSO) to 1 mL of particles; the particles were kept at room temperature for 2 h prior to being centrifuged to remove unreacted dye. Fluorescently labeled particles were stored in 0.5× D-PBS at 4 °C. Particles larger than ~400 nm in diameter were removed *via* size exclusion chromatography or differential centrifugation before cargo loading and liposome fusion; ~5% of the total mass of particles (mostly >1 $\mu$m in diameter) was retained upon fractionation.

**Characterization of Silica Nanoparticles.** A JEOL 2010 High Resolution Transmission Electron Microscope (JEOL, Ltd.; Carlsbad, CA) and a Hitachi S-5200 Scanning Electron Microscope (Hitachi High-Technologies Corporation; Tokyo, Japan) were used to image the mesoporous silica particles. For TEM imaging, particles were dispersed in ethanol at a concentration of 5 mg/mL, and 4 $\mu$L of this solution was transferred onto a holey carbon-coated copper TEM grid (SPI Supplies; West Chester, PA). Excess liquid was wicked off using a Kim wipe, and the grid was allowed to dry before imaging at 200 kV. For SEM imaging, grids were prepared as described above and imaged at 2 kV and 10 $\mu$A. Dynamic light scattering of mesoporous silica nanoparticles, as well as cargo-loaded protocells and lipid nanoparticles, was performed using a Zetasizer Nano (Malvern; Worcestershire, United Kingdom). Samples were prepared by diluting 48 $\mu$L of silica particles (25 mg/mL) in 2.4 mL of 0.5× D-PBS. Solutions were transferred to 1 mL polystyrene cuvettes (Sarstedt; Nümbrecht, Germany) for analysis. Zeta potential measurements were made using a Zetasizer Nano (Malvern; Worcestershire, United Kingdom). Silica particles were diluted 1:50 in 0.5× D-PBS and transferred to 1 mL folded capillary cells (Malvern; Worcestershire, United Kingdom) for analysis. Nitrogen sorption was performed using an ASAP 2020 surface area and porosity analyzer (Micromeritics Instrument Corporation; Norcross, GA, USA); surface area was determined using the Brunauer−Emmett−Teller model, and the cumulative pore volume plot was calculated from the adsorption branch of the isotherm using the Barrett−Joyner−Halenda model. Pore size is defined as the Kelvin diameter plus the statistical thickness of the adsorbed film.

**Liposome Fusion to Mesoporous Silica Nanoparticles.** The procedure used to synthesize protocells has been described previously[31,34,58,59] and will be mentioned only briefly. Lipids were ordered from Avanti Polar Lipids predissolved in chloroform and stored at −20 °C. Immediately prior to protocell synthesis, 2.5 mg of lipid was dried under a stream of nitrogen and placed in a vacuum oven (model 1450M, VWR International, West Chester, PA, USA) overnight to remove residual solvent. Lipids were rehydrated in 0.5× D-PBS at a concentration of 2.5 mg/mL and were passed through a 100 nm filter at least 10 times using a Mini-Extruder set (Avanti Polar Lipids, Inc.; Alabaster, AL, USA). Resulting liposomes (~120 nm in diameter) were stored at 4 °C for no more than one week. Mesoporous silica cores (25 mg/mL) were incubated with a 2- to 4-fold volumetric excess of liposomes for 30−90 min at room temperature. Protocells were stored in the presence of excess lipid for up to 1 month at 4 °C. To remove excess lipid, protocells were centrifuged at 5000 rpm for 1 min, washed twice, and resuspended in 0.5× D-PBS.

Lipids were lyophilized together prior to rehydration and extrusion; for example 75 $\mu$L of DOPC (25 mg/mL), 5 $\mu$L of DOPE (25 mg/mL), 10 $\mu$L of cholesterol (75 mg/mL), and 10 $\mu$L of 18:1 PEG−2000 PE (25 mg/mL) were combined and dried to form liposomes composed of DOPC with 5 wt % DOPE, 30 wt % cholesterol, and 10 wt % PEG−2000. A DOPC:DOPE:cholesterol:18:1 PEG−2000 PE mass ratio of 55:5:30:10 was used to synthesize "DOPC protocells", while a DOTAP:DOPE:cholesterol:18:1 PEG−2000 PE mass ratio of 55:5:30:10 was used to synthesize "DOTAP protocells".

**Conjugation of Peptides to the Supported Lipid Bilayer.** SP94 and H5WYG peptides, synthesized with C-terminal cysteine residues, were conjugated to primary amines present in the head groups of PE using the heterobifunctional cross-linker SM $(PEG)_{24}$, which is reactive toward sulfhydryl and amine moieties and possesses a 9.52 nm PEG spacer arm. Protocells were first incubated with a 10-fold molar excess of $SM(PEG)_{24}$ for 2 h at room temperature and centrifuged (1 min at 5000 rpm) to remove unreacted cross-linker. Activated protocells were then incubated with a 5-fold molar excess of SP94 for 2 h at room temperature to attain a peptide density of 0.015 wt % (~6 peptides/protocell) and with a 500-fold molar excess of H5WYG for 4 h at room temperature to attain a peptide density of 0.500 wt % (~240 peptides/protocell). Protocells were washed to remove free peptide, and average peptide density was determined by Tricine-SDS-PAGE, as described previously.[31]

**Synthesis of siRNA-Loaded Protocells.** AEPTMS-modified cores (25 mg/mL) were soaked in siRNA (250 $\mu$M in 1× D-PBS) for 2 h at 4 °C. Unencapsulated cargo was removed *via* centrifugation at 5000 rpm for 1 min, and DOPC liposomes were immediately fused to cargo-loaded cores as described above. Unmodified cores were loaded with siRNA *via* the synergistic mechanism previously described by us.[34] Briefly, 25 $\mu$L of siRNA (1 mM) was added to 75 $\mu$L of silica nanoparticles (25 mg/mL). The solution was gently vortexed and incubated with 200 $\mu$L of DOTAP liposomes overnight at 4 °C. Excess lipid and unencapsulated siRNA were removed *via* centrifugation immediately before use.

**Synthesis of siRNA-Loaded Lipid Nanoparticles.** To prepare siRNA-loaded DOPC lipid nanoparticles, DOPC, DOPE, cholesterol, and 18:1 PEG−2000 PE were first mixed in a 55:5:30:10 mass ratio, dried under a stream of nitrogen, and placed in a vacuum oven overnight to remove residual chloroform. The lipid film was then dissolved in *tert*-butanol and mixed 1:1 (v/v) with a siRNA solution (diluted in 10 mM Tris-HCl (pH 7.4) with 0.85% (w/v) NaCl and 0.25 M sucrose) such that the final DOPC:siRNA ratio was 10:1 (w/w). The mixture was vortexed, flash frozen in a bath of acetone and dry ice, and lyopholized. Immediately before use, the LNP preparation was hydrated with an isotonic sucrose solution (10 mM Tris-HCl (pH 7.4) with 0.85% (w/v) NaCl and 0.25 M sucrose) to a final siRNA concentration of 100 $\mu$g/mL; unencapsulated siRNA was removed *via* centrifugal-driven filtration (10 kDa MWCO).

We prepared siRNA-loaded DOTAP LNPs as described by Wu *et al.*,[60] with minor modifications. We replaced PEGylated ceramide with 18:1 PEG−2000 PE and used a DOTAP:DOPE: cholesterol:PEG−2000 PE ratio of 55:5:30:10. We, additionally, dissolved lyopholized LNPs in 10 mM Tris-HCl (pH 7.4) with 0.85% (w/v) NaCl and 0.25 M sucrose to a final siRNA concentration of 100 $\mu$g/mL and removed unencapsulated siRNA using a centrifugal filtration device (10 kDa MWCO). LNPs were dissolved in 0.5× D-PBS for zeta potential analysis.

To modify DOTAP LNPs with SP94 and H5WYG, they were first incubated with a 10-fold molar excess of $SM(PEG)_{24}$ for 2 h at room temperature; after removal of unreacted cross-linker *via* centrifugal-driven filtration (10 kDa MWCO), they were incubated with a 5-fold molar excess of SP94 and a 1000-fold molar excess of H5WYG for 2 h at room temperature. Free peptide was removed using a centrifugal filtration device (10 kDa MWCO).

**Determination of Cargo Capacities and Release Rates.** The capacities of protocells and lipid nanoparticles for siRNA was determined by incubating $1 \times 10^{10}$ particles in 1 wt % SDS (dissolved in D-PBS) for 24 h and centrifuging the solutions to remove protocell cores and other debris. The concentration of siRNA in the supernatant was determined by comparing the absorbance at 260 nm to a standard curve.

The rate of siRNA release under neutral and acidic pH conditions was determined by suspending $1 \times 10^{10}$ particles in 1 mL of a simulated body fluid (EMEM with 150 mM NaCl and 10% serum, pH 7.4) or citric acid buffer (pH 5.0) for various periods of time at 37 °C. Particles were pelleted *via* centrifugation (5 min at 5000*g* for protocells and 30 min at 15000*g* for LNPs; Microfuge 16 centrifuge; Beckman-Coulter; Brea, CA, USA). siRNA concentrations in the supernatant were determined using UV−visible spectroscopy, as described above. The concentration of released cargo was converted into a percentage of the cargo concentration that was initially encapsulated within $10^{10}$ particles.

**Quantification of Cyclin A2, B1, D1, and E Protein Expression.** To determine the concentration of siRNA necessary to silence 90% of cyclin A2, cyclin B1, cyclin D1, or cyclin E expression ($IC_{90}$, see Figure 4A), $1 \times 10^6$ Hep3B cells were exposed to various concentrations of siRNA loaded in SP94-targeted DOPC protocells for 48 h at 37 °C. Cells were then harvested by gentle shaking in 5 mM EDTA for 30 min at 37 °C, centrifuged (1000 rpm, 1 min) to remove excess particles, fixed with 3.7% formaldehyde (15 min at room temperature), and permeabilized with 0.2% Triton X-100 (5 min at room temperature); cells were then exposed to a 1:500 dilution of anticyclin A2, anticyclin B1, anticyclin D1, or anticyclin E, labeled using an Alexa Fluor 488 antibody labeling kit, for 1 h at 37 °C. Cells were washed three times and resuspended in D-PBS for flow cytometry analysis (FACSCalibur). GraphPad Prism (GraphPad Software, Inc.; La Jolla, CA, USA) was employed to calculate $IC_{90}$ values from plots of log(siRNA concentration) *versus* mean fluorescence intensity; the initial protein concentration was taken to be the mean fluorescence intensity of antibody-labeled cells prior to treatment with siRNA-loaded protocells.

To determine the time-dependent decrease in cyclin A2, cyclin B1, cyclin D1, and cyclin E expression (see Figure 4B), siRNA-loaded, SP94-targeted DOPC protocells were mixed with $1 \times 10^6$ Hep3B cells such that the final siRNA concentration was 125 pM; cells and protocells were incubated at 37 °C for various periods of time, and resulting protein levels were determined *via* immunofluorescence as described above. The same process was used to quantify cyclin levels in Hep3B treated with free siRNA, siRNA-loaded DOTAP LNPs, and SP94-targeted protocells loaded with Silencer Select negative control siRNA (see the Supplementary Figures 2 and 3); the total siRNA concentration was maintained at 125 pM in all time-dependent experiments.

The dose- and time-dependent decreases in cyclin A2 mRNA (Figure 4A and B, respectively) were determined by incubating Hep3B with SP94-targeted protocells loaded with the cyclin A2-specific siRNA as described above. Cells were washed three times with cold 1× PBS to remove excess protocells. mRNA was then isolated from cells and converted to cDNA using the TaqMan Fast Cells-to-CT kit. Quantitative PCR was performed by SeqWright, Inc. (Houston, TX, USA).

To collect the data depicted in Figure 4C (left axis), a sufficient volume of siRNA-loaded, SP94-targeted DOPC protocells or DOTAP LNPs was added to $1 \times 10^6$ Hep3B or hepatocytes such that the final siRNA concentration was 125 pM. Samples were incubated at 37 °C for 48 h, and the resulting decrease in cyclin A2 expression was quantified as described above. To determine the values plotted in Figure 4C (right axis), $1 \times 10^6$ Hep3B cells were exposed to various concentrations (particles/mL) of siRNA-loaded, SP94-targeted DOPC protocells or DOTAP LNPs for 48 h at 37 °C; cyclin A2 expression was quantified using immunofluorescence, and the number of particles necessary to reduce cyclin A2 expression by 90% was calculated from a plot of particle concentration *versus* cyclin A2 concentration.

Cells depicted in Figure 5 were exposed to a 10-fold excess of siRNA-loaded, SP94-targeted DOPC protocells with Alexa Fluor 647-labeled cores for either 1 or 48 h at 37 °C. Cells were washed three times with D-PBS, labeled with Hoechst 33342 per the manufacturer's instructions, fixed with 3.7% formaldehyde (15 min at room temperature), permeabilized with 0.2% Triton X-100 (5 min at room temperature), and blocked with Image-iT FX signal enhancer (30 min, room temperature). Cells were then exposed to Alexa Fluor 488-labeled antibodies against cyclin A2, B1, D1, or E (diluted 1:500 in 1% BSA) overnight at 4 °C, washed three times in D-PBS, and mounted with SlowFade Gold.

**Quantification of Growth Arrest.** The numbers of proliferating and growth arrested Hep3B cells (Figure 6A and B, respectively) were determined by first exposing $1 \times 10^6$ cells to SP94-targeted, siRNA-loaded protocells for various periods of time at 37 °C; protocells were loaded with a siRNA cocktail specific for cyclins A2, B1, D1, and E, and the total siRNA concentration was maintained at ~125 pM. Cells were then washed three times in 1× PBS to remove excess protocells. To determine the percentage of proliferating Hep3B, protocell-treated cells were incubated with 10 $\mu$M BrdU (in complete growth medium) for 12 h at 37 °C, harvested by gentle shaking in 5 mM EDTA for 30 min at 37 °C, and fixed with 4% formaldehyde for 30 min at 4 °C. Cells were then washed three times in 1× PBS with 0.1% Triton X-100, incubated in 1 N HCl for 10 min on ice, incubated in 2 N HCl for 10 min at room temperature and then 20 min at 37 °C, incubated in 0.1 M borate for 12 min at room temperature, and washed three times in 1× PBS with 0.1% Triton X-100. Cells were blocked in 1× PBS with 0.1% Triton X-100, 1 M glycine, and 5% goat serum for 1 h at room temperature and then incubated with an Alexa Fluor 488-labeleled mouse monoclonal antibody to BrdU (1:100 dilution in 1× PBS with 1% BSA) overnight at 4 °C. Cells were washed three times with 1× PBS, and the number of cells positive for BrdU incorporation was determined using a FACSCalibur flow cytometer. Cells were considered positive if their mean fluorescence intensities (MFI) were 100 fluorescence units (FU) greater than the MFI of unlabeled cells. To determine the percentage of $G_0/G_1$ and $G_2/M$ arrested Hep3B, protocell-treated cells were harvested by gentle shaking in 5 mM EDTA for 30 min at 37 °C, incubated with 1 $\mu$g/mL of Hoechst 33342 for 15 min at 37 °C, washed three times with 1× PBS, and immediately analyzed using a MoFlo high-performance cell sorter (Dako-Cytomation; Carpinteria, CA, USA) equipped with Dako-Cytomation's SUMMIT software, version 4.3.01. Cells were detected using a 488 nm Innova 90 laser (Coherent Inc.; Santa Clara, CA, USA), and a gate was placed on the forward scatter-side scatter plot that excluded cellular debris. Hoechst 33342 was excited with a 355 nm Innova 90 laser, and emission intensity was collected in the FL-6 channel (450/65 filter/bandpass). Single cells were gated using width and area parameters; the area parameter histogram was used to determine the percentage of gated cells in $G_0/G_1$, S, and $G_2/M$ phases. Data were acquired with the SSC channel in log mode and all other channels in linear mode.

**Quantification of Apoptosis.** The time-dependent viability of Hep3B and hepatocytes (see Figure 6C) exposed to siRNA-loaded, SP94-targeted protocells was determined by incubating $1 \times 10^6$ cells with 125 pM siRNA for various periods of time at 37 °C. Cells were harvested by gentle shaking in 5 mM EDTA for 30 min at 37 °C, centrifuged (1000 rpm, 1 min) to remove excess protocells, and stained with Alexa Fluor 488-labeled annexin V and propidium iodide per the manufacturer's instructions. The numbers of viable (double-negative) and nonviable (single- or double-positive) cells were determined *via* flow cytometry (FACSCalibur). Voltages were established using (1) untreated, unlabeled Hep3B (100% of cells were contained within the lower left quadrant, spanning from $10^0$ to $10^2$ fluorescence units on the FL-1 and FL-2 axes); (2) Hep3B transfected with the cyclin-specific siRNA cocktail using Lipofectamine RNAiMAX and singly stained with Alexa Fluor 488-labeled annexin V (96% of cells were contained within the lower right quadrant, spanning from $10^2$ to $10^4$ FUs on the FL-1 axis and $10^0$ to $10^2$ FUs on the FL-2 axis); and (3) Hep3B transfected with the cyclin-specific siRNA cocktail using Lipofectamine RNAiMAX and singly stained with propidium iodide (98% of cells were contained within the upper right quadrant, spanning from $10^0$ to $10^2$ FUs on the FL-1 axis and $10^2$ to $10^4$ FUs on the FL-2 axis). Cells were transfected according to Invitrogen's "reverse transfection" protocol with an initial cell concentration of $5 \times 10^5$ (seeded in 60 mm plates), a final siRNA concentration of 50 nM, and a total incubation time of 72 h.

To collect the data depicted in Figure 6D (left axis), a sufficient volume of siRNA-loaded, SP94-targeted DOPC protocells or DOTAP LNPs was added to $1 \times 10^6$ Hep3B or hepatocytes such that the final siRNA concentration was 125 pM. Samples were incubated at 37 °C for 48 h, and the number of apoptotic cells was determined as described above. To determine the values plotted in Figure 6D (right axis), $1 \times 10^6$ Hep3B cells were exposed to various concentrations (particles/mL) of siRNA-loaded, SP94-targeted DOPC protocells or DOTAP LNPs for 48 h at 37 °C; the number of apoptotic Hep3B was quantified using the annexin V/propidium iodide assay.

Cells shown in Figure 7 were exposed to a 10-fold excess of siRNA-loaded, SP94-targeted protocells with Alexa Fluor 647-labeled cores for either 1 or 48 h at 37 °C. Cells were then washed three times with D-PBS, stained with Hoechst 33342, Alexa Fluor 488-labeled annexin V, and propidium iodide per the manufacturer's instructions, fixed (3.7% formaldehyde for 10 min at room temperature), and mounted with SlowFade Gold.

To collect the data depicted in Supplementary Figure 1, $1 \times 10^6$ Hep3B cells were incubated with $1 \times 10^9$ AEPTMS-modified multimodal silica nanoparticles, DOPC protocells with AEPTMS-modified cores, or DOTAP LNPs, all loaded with Silencer Select negative control siRNA for 48 h at 37 °C. Cells were then washed three times with 1× PBS to remove excess particles and stained with propidium iodide, per the manufacturer's instructions. Cells were immediately analyzed *via* flow cytometry; cells were considered positive if their mean fluorescence intensities were 100 fluorescence units greater than the MFI of unlabeled cells.

**Flow Cytometry Equipment and Settings.** For Figures 4A–C and 6A, C, and D, as well as Supplementary Figures 1–3, cell samples were analyzed with a FACSCalibur flow cytometer (Becton Dickinson; Franklin Lakes, NJ, USA) equipped with BD CellQuest software, version 5.2.1. Samples were acquired with the fsc channel in linear mode, and all other channels in log mode. Events were triggered on the basis of forward light scatter, and, for data depicted in Figure 4 and Supplementary Figures 2 and 3, a gate was placed on the forward scatter-side scatter plot that excluded cellular debris. Alexa Fluor 488 was excited using the 488 nm laser source, and emission intensity was collected in the FL1 channel (530/30 filter/bandpass). Propidium iodide was excited using the 488 nm laser source, and emission intensity was collected in the FL2 channel (585/42). Mean fluorescence intensity was determined using FlowJo software, version 6.4 (Tree Star, Inc.; Ashland, OR, USA). All plots were generated using Sigma Plot, version 11.0 (Systat Software, Inc.; San Jose, CA, USA).

**Fluorescence Microscopy Equipment and Settings.** Three- and four-color images were acquired using a Zeiss LSM510 META (Carl Zeiss MicroImaging, Inc.; Thornwood, NY, USA) operated in channel mode of the LSM510 software; a 63×, 1.4-NA oil immersion objective was employed in all imaging. Typical laser power settings were 10% transmission for the 405 nm diode laser, 5% transmission (50% output) for the 488 nm argon laser, 100% transmission for the 543 nm HeNe laser, and 80% transmission for the 633 nm HeNe laser. Gain and offset were adjusted for each channel to avoid saturation and were typically maintained at 500–700 and −0.1, respectively. 8-Bit z-stacks with 1024 × 1024 resolution were acquired with a 1.0 $\mu$m optical slice. LSM510 and Zen 2009 Light Edition software were used to overlay channels and to create collapsed projections of z-stack images. All fluorescence images are collapsed projections.

For all microscopy experiments, cells were grown in culture flasks to 70–80% confluence, harvested (0.05% trypsin, 10 min), centrifuged at 4000 rpm for 2 min, and resuspended in complete growth medium. Cells at a volume of $1 \times 10^4$ to $1 \times 10^6$ cells/mL were seeded on sterile coverslips (25 mm, No. 1.5) coated with 0.01% poly-L-lysine (150–300 kDa) and allowed to adhere for 4–24 h at 37 °C before being exposed to protocells. Forty-eight-hour samples were spun back onto coverslips using a Cytopro Centrifuge, model 7620 (Wescor, Inc.; Logan, UT, USA).

*Conflict of Interest:* The authors declare no competing financial interest.

*Acknowledgment.* This work was supported by the NIH/Roadmap for Medical Research under grant PHS 2 PN2 EY016570B; NCI Cancer Nanotechnology Platform Partnership grant 1U01CA151792-01; the Air Force Office of Scientific Research grant FA 9550-07-1-0054/9550-10-1-0054; the U.S. Department of Energy, Office of Basic Energy Sciences, Division of Materials Sciences and Engineering; Sandia National Laboratories' Laboratory Directed Research and Development (LDRD) program; the UCLA Center for Nanobiology and Predictive Toxicology (NIEHS grant 1U19ES019528-01); and the NSF ERC Center for Environmental Implications of Nanotechnology at UCLA (NSF:EF-0820117). C.E.A. was supported by IGERT Fellowship Grant NSF DGE-0504276 and the President Harry S. Truman Fellowship in National Security Science and Engineering at Sandia National Laboratories. E.C.C. was supported by NSF IGERT grant DGE-0549500. We thank Nick Carroll and Dimiter Petsev for their assistance with nanoparticle synthesis, Darren Dunphy for his help with nanoparticle characterization, Mona Aragon for generating the schematic, and Carol Ashley for performing final edits of the manuscript. Images in this paper were generated in the University of New Mexico Cancer Center Fluorescence Microscopy Facility, supported by NCRR, NSF, and NCI as detailed at http://hsc.unm.edu/crtc/microscopy/Facility.html. Data were generated in the Flow Cytometry Shared Resource Center supported by the University of New Mexico Health Sciences Center and the University of New Mexico Cancer Center. Sandia is a multiprogram laboratory operated by Sandia Corporation, a wholly owned subsidiary of Lockheed Martin Company, for the U.S. Department of Energy's National Nuclear Security Administration under contract DE-AC04-94AL85000.

*Supporting Information Available:* Dose- and time-dependent effects of free cyclin-specific siRNAs, DOTAP lipid nanoparticles loaded with cyclin-specific siRNAs, and DOPC protocells loaded with Silencer Select negative control siRNA on cyclin protein concentrations; viability of Hep3B cells exposed to AEPTMS-modified silica nanoparticles, DOPC protocells with AEPTMS-modified cores, and DOTAP lipid nanoparticles. This material is available free of charge *via* the Internet at http://pubs.acs.org.

## REFERENCES AND NOTES

1. Peer, D.; Karp, J. M.; Hong, S.; Farokhzad, O. C.; Margalit, R.; Langer, R. Nanocarriers as an Emerging Platform for Cancer Therapy. *Nat. Nanotechnol.* **2007**, *2*, 751–760.
2. Petros, R. A.; DeSimone, J. M. Strategies in the Design of Nanoparticles for Therapeutic Applications. *Nat. Rev. Drug Discovery* **2010**, *9*, 615–627.
3. Wang, M.; Thanou, M. Targeting Nanoparticles to Cancer. *Pharm. Res.* **2010**, *62*, 90–99.

4. Meister, G.; Tuschl, T. Mechanisms of Gene Silencing by Double-Stranded RNA. *Nature* **2004**, *431*, 343–349.
5. Rana, T. M. Illuminating the Silence: Understanding the Structure and Function of Small RNAs. *Nat. Rev. Mol. Cell Biol.* **2007**, *8*, 23–36.
6. Davidson, B. L.; McCray, P. B. Current Prospects for RNA Interference-Based Therapies. *Nat. Rev. Genet.* **2011**, *12*, 329–340.
7. Lares, M. R.; Rossi, J. J.; Ouellet, D. L. RNAi and Small Interfering RNAs in Human Disease Therapeutic Applications. *Trends Biotechnol.* **2010**, *28*, 570–579.
8. Bumcrot, D.; Manoharan, M.; Koteliansky, V.; Sah, D. W. Y. RNAi Therapeutics: A Potential New Class of Pharmaceutical Drugs. *Nat. Chem. Biol.* **2006**, *2*, 711–719.
9. Aagaard, L.; Rossi, J. J. RNAi Therapeutics: Principles, Prospects and Challenges. *Adv. Drug Delivery Rev.* **2007**, *59*, 75–86.
10. Ozpolat, B.; Sood, A. K.; Lopez-Berestein, G. Nanomedicine Based Approaches for the Delivery of siRNA in Cancer. *J. Intern. Med.* **2010**, *267*, 44–53.
11. Petrocca, F.; Lieberman, J. Promise and Challenge of RNA Interference-Based Therapy for Cancer. *J. Clin. Oncol.* **2011**, *29*, 747–754.
12. de Fougerolles, A.; Vornlocher, H.-P.; Maraganore, J.; Lieberman, J. Interfering with Disease: A Progress Report on siRNA-Based Therapeutics. *Nat. Rev. Drug Discovery* **2007**, *6*, 443–453.
13. Davis, M. E.; Zuckerman, J. E.; Choi, C. H. J.; Seligson, D.; Tolcher, A.; Alabi, C. A.; Yen, Y.; Heidel, J. D.; Ribas, A. Evidence of RNAi in Humans from Systemically Administered siRNA via Targeted Nanoparticles. *Nature* **2010**, *464*, 1067–1070.
14. Jackson, A. L.; Burchard, J.; Leake, D.; Reynolds, A.; Schelter, J.; Guo, J.; Johnson, J. M.; Lim, L.; Karpilow, J.; Nichols, K.; *et al.* Position-Specific Chemical Modification of siRNAs Reduces "Off-Target" Transcript Silencing. *RNA* **2006**, *12*, 1197–1205.
15. Judge, A. D.; Sood, V.; Shaw, J. R.; Fang, D.; McClintock, K.; MacLachlan, I. Sequence-Dependent Stimulation of the Mammalian Innate Immune Response by Synthetic siRNA. *Nat. Biotechnol.* **2005**, *23*, 457–462.
16. Soutschek, J.; Akinc, A.; Bramlage, B.; Charisse, K.; Constien, R.; Donoghue, M.; Elbashir, S.; Geick, A.; Hadwiger, P.; Harborth, J.; *et al.* Therapeutic Silencing of an Endogenous Gene by Systemic Administration of Modified siRNAs. *Nature* **2004**, *432*, 173–178.
17. Pecot, C. V.; Calin, G. A.; Coleman, R. L.; Lopez-Berestein, G.; Sood, A. K. RNA Interference in the Clinic: Challenges and Future Directions. *Nat. Rev. Cancer* **2011**, *11*, 59–67.
18. Whitehead, K. A.; Langer, R.; Anderson, D. G. Knocking Down Barriers: Advances in siRNA Delivery. *Nat. Rev. Drug Discovery* **2009**, *8*, 129–138.
19. Edbrooke, M.; Clarke, N. RNAi Therapeutics: Addressing Targets? *Eur. Pharm. Rev.* **2008**, *4*, 11–17.
20. Cauda, V.; Argyo, C.; Bein, T. Impact of Different Pegylation Patterns on the Long-Term Bio-Stability of Colloidal Mesoporous Silica Nanoparticles. *J. Mater. Chem.* **2010**, *20*, 8693–8699.
21. Cauda, V.; Argyo, C.; Schlossbauer, A.; Bein, T. Controlling the Delivery Kinetics from Colloidal Mesoporous Silica Nanoparticles with pH-Sensitive Gates. *J. Mater. Chem.* **2010**, *20*, 4305–4311.
22. Cauda, V.; Engelke, H.; Sauer, A.; Arcizet, D.; Bräuchle, C.; Rädler, J.; Bein, T. Colchicine-Loaded Lipid Bilayer-Coated 50 nm Mesoporous Nanoparticles Efficiently Induce Microtubule Depolymerization Upon Cell Uptake. *Nano Lett.* **2010**, *10*, 2484–2492.
23. Cauda, V.; Muehistein, L.; Onida, B.; Bein, T. Tuning Drug Uptake and Release Rates through Different Morphologies and Pore Diameters of Confined Mesoporous Silica. *Microporous Mesoporous Mater.* **2009**, *118*, 435–442.
24. Cauda, V.; Schlossbauer, A.; Bein, T. Bio-Degradation Study of Colloidal Mesoporous Silica Nanoparticles: Effect of Surface Functionalization with Organo.Silanes and Poly-(Ethylene Glycol). *Microporous Mesoporous Mater.* **2010**, *132*, 60–71.
25. Hom, C.; Lu, J.; Liong, M.; Luo, H.; Li, Z.; Zink, J. I.; Tamanoi, F. Mesoporous Silica Nanoparticles Facilitate Delivery of siRNA to Shutdown Signaling Pathways in Mammalian Cells. *Small* **2010**, *6*, 1185–1190.
26. Liong, M.; Lu, J.; Kovochich, M.; Xia, T.; Ruehm, S. G.; Nel, A. E.; Tamanoi, F.; Zink, J. I. Multifunctional Inorganic Nanoparticles for Imaging, Targeting, and Drug Delivery. *ACS Nano* **2008**, *2*, 889–896.
27. Meng, H.; Liong, M.; Xia, T.; Li, Z.; Ji, Z.; Zink, J. I.; Nel, A. E. Engineered Design of Mesoporous Silica Nanoparticles to Deliver Doxorubicin and P-Glycoprotein siRNA to Overcome Drug Resistance in a Cancer Cell Line. *ACS Nano* **2010**, *4*, 4539–4550.
28. Meng, H.; Xue, M.; Xia, T.; Zhao, Y.-L.; Tamanoi, F.; Stoddart, J. F.; Zink, J. I.; Nel, A. E. Autonomous in Vitro Anticancer Drug Release from Mesoporous Silica Nanoparticles by pH-Sensitive Nanovalves. *J. Am. Chem. Soc.* **2010**, *132*, 12690–12697.
29. Sauer, A. M.; Schlossbauer, A.; Ruthardt, N.; Cauda, V.; Bein, T.; Bräuchle, C. Role of Endosomal Escape for Disulfide-Based Drug Delivery from Colloidal Mesoporous Silica Evaluated by Live-Cell Imaging. *Nano Lett.* **2010**, *10*, 3684–3691.
30. Xia, T.; Kovochich, M.; Liong, M.; Meng, H.; Kabehie, S.; George, S.; Zink, J. I.; Nel, A. E. Polyethyleneimine Coating Enhances the Cellular Uptake of Mesoporous Silica Nanoparticles and Allows Safe Delivery of siRNA and DNA Constructs. *ACS Nano* **2009**, *3*, 3273–3286.
31. Ashley, C. E.; Carnes, E. C.; Phillips, G. K.; Padilla, D.; Durfee, P. N.; Brown, P. A.; Hanna, T. N.; Liu, J.; Phillips, B.; Carter, M. B.; *et al.* The Targeted Delivery of Multicomponent Cargos to Cancer Cells by Nanoporous Particle-Supported Lipid Bilayers. *Nat. Mater.* **2011**, *10*, 389–397.
32. Carroll, N. J.; Pylypenko, S.; Atanassov, P. B.; Petsev, D. N. Microparticles with Bimodal Nanoporosity Derived by Microemulsion Templating. *Langmuir* **2009**, *25*, 13540–13544.
33. Zhang, S.; Zhao, B.; Jiang, H.; Wang, B.; Ma, B. Cationic Lipids and Polymers Mediated Vectors for Delivery of siRNA. *J. Controlled Release* **2007**, *123*, 1–10.
34. Liu, J.; Stace-Naughton, A.; Jiang, X.; Brinker, C. J. Porous Nanoparticle Supported Lipid Bilayers (Protocells) as Delivery Vehicles. *J. Am. Chem. Soc.* **2009**, *131*, 1354–1355.
35. Pines, J. Cyclins: Wheels within Wheels. *Cell Growth Di⊠er.* **1991**, *2*, 305–310.
36. Grimm, D.; Kay, M. A. Therapeutic Application of RNAi: Is mRNA Targeting Finally Ready for Prime Time? *J. Clin. Invest.* **2007**, *117*, 3633–3641.
37. Chen, Y.; Bathula, S. R.; Li, J.; Huang, L. Multifunctional Nanoparticles Delivering Small Interfering RNA and Doxorubicin Overcome Drug Resistance in Cancer. *J. Biol. Chem.* **2010**, *285*, 22639–22650.
38. Li, S.-D.; Chen, Y.-C.; Hackett, M. J.; Huang, L. Tumor-Targeted Delivery of siRNA by Self-Assembled Nanoparticles. *Mol. Ther.* **2007**, *16*, 163–169.
39. Howard, K. A.; Rahbek, U. L.; Liu, X.; Damgaard, C. K.; Glud, S. Z.; Andersen, M. O.; Hovgaard, M. B.; Schmitz, A.; Nyengaard, J. R.; Besenbacher, F.; *et al.* RNA Interference in Vitro and in Vivo Using a Chitosan/siRNA Nanoparticle System. *Mol. Ther.* **2006**, *14*, 476–484.
40. Hu-Lieskovan, S.; Heidel, J. D.; Bartlett, D. W.; Davis, M. E.; Triche, T. J. Sequence-Specific Knockdown of Ews-Fli1 by Targeted, Nonviral Delivery of Small Interfering RNA Inhibits Tumor Growth in a Murine Model of Metastatic Ewing's Sarcoma. *Cancer Res.* **2005**, *65*, 8984–8992.
41. Schiffelers, R. M.; Ansari, A.; Xu, J.; Zhou, Q.; Tang, Q.; Storm, G.; Molema, G.; Lu, P. Y.; Scaria, P. V.; Woodle, M. C. Cancer siRNA Therapy by Tumor Selective Delivery with Ligand-Targeted Sterically Stabilized Nanoparticle. *Nucleic Acids Res.* **2004**, *32*, e149.
42. Cheng, H.; Zhu, J.-L.; Zeng, X.; Jing, Y.; Zhang, X.-Z.; Zhuo, R.-X. Targeted Gene Delivery Mediated by Folate-Polyethylenimine-Block-Poly(Ethylene Glycol) with Receptor Selectivity. *Bioconjugate Chem.* **2009**, *20*, 481–487.

43. DiFiglia, M.; Sena-Esteves, M.; Chase, K.; Sapp, E.; Pfister, E.; Sass, M.; Yoder, J.; Reeves, P.; Pandey, R. K.; Rajeev, K. G.; *et al*. Therapeutic Silencing of Mutant Huntingtin with siRNA Attenuates Striatal and Cortical Neuropathology and Behavioral Deficits. *Proc. Natl. Acad. Sci. U. S. A.* **2007**, *104*, 17204–17209.
44. Chen, Y.; Zhu, X.; Zhang, X.; Liu, B.; Huang, L. Nanoparticles Modified with Tumor-Targeting Scfv Deliver siRNA and miRNA for Cancer Therapy. *Mol. Ther.* **2010**, *18*, 1650–1656.
45. Orava, E. W.; Cicmil, N.; Gariépy, J. Delivering Cargoes into Cancer Cells Using DNA Aptamers Targeting Internalized Surface Portals. *Biochim. Biophys. Acta* **2010**, *1798*, 2190–2200.
46. Lv, H.; Zhang, S.; Wang, B.; Cui, S.; Yan, J. Toxicity of Cationic Lipids and Cationic Polymers in Gene Delivery. *J. Controlled Release* **2006**, *114*, 100–109.
47. Becker, A. L.; Orlotti, N. I.; Folini, M.; Cavalieri, F.; Zelikin, A. N.; Johnston, A. P. R; Zaffaroni, N.; Caruso, F. Redox-Active Polymer Microcapsules for the Delivery of a Survivin-Specific siRNA in Prostate Cancer Cells. *ACS Nano* **2011**, *5*, 1335–1344.
48. MacDiarmid, J. A.; Amaro-Mugridge, N. B.; Madrid-Weiss, J.; Sedliarou, I.; Wetzel, S.; Kochar, K.; Brahmbhatt, V. N.; Phillips, L.; Pattison, S. T.; Petti, C.; *et al*. Sequential Treatment of Drug-Resistant Tumors with Targeted Minicells Containing siRNA or a Cytotoxic Drug. *Nat. Biotechnol.* **2009**, *27*, 643–651.
49. Tanaka, T.; Mangala, L. S.; Vivas-Mejia, P. E.; Nieves-Alicea, R.; Mann, A. P.; Mora, E.; Han, H. D.; Shahzad, M. M.; Liu, X.; Bhavane, R.; *et al*. Sustained Small Interfering RNA Delivery by Mesoporous Silicon Particles. *Cancer Res.* **2010**, *70*, 3687–3696.
50. Li, J.; Chen, Y.-C.; Tseng, Y.-C.; Mozumdar, S.; Huang, L. Biodegradable Calcium Phosphate Nanoparticle with Lipid Coating for Systemic siRNA Delivery. *J. Controlled Release* **2010**, *142*, 416–421.
51. Li, S.-D.; Huang, L. Targeted Delivery of Antisense Oligodeoxynucleotide and Small Interference RNA into Lung Cancer Cells. *Mol. Pharmaceutics* **2006**, *3*, 579–588.
52. Pirollo, K. F.; Rait, A.; Zhou, Q.; Hwang, S. H.; Dagata, J. A.; Zon, G.; Hogrefe, R. I.; Palchik, G.; Chang, E. H. Materializing the Potential of Small Interfering RNA via a Tumor-Targeting Nanodelivery System. *Cancer Res.* **2007**, *67*, 2938–2943.
53. Sun, T.-M.; Du, J.-Z.; Yao, Y.-D.; Mao, C.-Q.; Dou, S.; Huang, S.-Y.; Zhang, P.-Z.; Leong, K. W.; Song, E.-W.; Wang, J. Simultaneous Delivery of siRNA and Paclitaxel via a "Two-in-One" Micelleplex Promotes Synergistic Tumor Suppression. *ACS Nano* **2011**, *5*, 1483–1494.
54. Xiong, X.-B.; Lavasanifar, A. Traceable Multifunctional Micellar Nanocarriers for Cancer-Targeted Co-Delivery of Mdr-1 siRNA and Doxorubicin. *ACS Nano* **2011**, *5*, 5202–5213.
55. Chen, Y.; Bathula, S. R.; Yang, Q.; Huang, L. Targeted Nanoparticles Deliver siRNA to Melanoma. *J. Invest. Dermatol.* **2010**, *130*, 2790–2798.
56. Chono, S.; Li, S.-D.; Conwell, C. C.; Huang, L. An Efficient and Low Immunostimulatory Nanoparticle Formulation for Systemic siRNA Delivery to the Tumor. *J. Controlled Release* **2008**, *131*, 64–69.
57. Bhattarai, S.; Muthuswamy, E.; Wani, A.; Brichacek, M.; Castañeda, A.; Brock, S.; Oupicky, D. Enhanced Gene and siRNA Delivery by Polycation-Modified Mesoporous Silica Nanoparticles Loaded with Chloroquine. *Pharm. Res.* **2010**, *27*, 2556–2568.
58. Liu, J. W.; Jiang, X. M.; Ashley, C.; Brinker, C. J. Electrostatically Mediated Liposome Fusion and Lipid Exchange with a Nanoparticle-Supported Bilayer for Control of Surface Charge, Drug Containment, and Delivery. *J. Am. Chem. Soc.* **2009**, *131*, 7567–7569.
59. Liu, J. W.; Stace-Naughton, A.; Brinker, C. J. Silica Nanoparticle Supported Lipid Bilayers for Gene Delivery. *Chem. Commun. (Cambridge, U.K.)* **2009**, 5100–5102.
60. Wu, S. Y.; Singhania, A.; Burgess, M.; Putral, L. N.; Kirkpatrick, C.; Davies, N. M.; McMillan, N. A. J. Systemic Delivery of E6/7 siRNA Using Novel Lipidic Particles and Its Application with Cisplatin in Cervical Cancer Mouse Models. *Gene Ther.* **2011**, *18*, 14–22.
61. Lo, A.; Lin, C.-T.; Wu, H.-C. Hepatocellular Carcinoma Cell-Specific Peptide Ligand for Targeted Drug Delivery. *Mol. Cancer Ther.* **2008**, *7*, 579–589.
62. Moore, N. M.; Sheppard, C. L.; Barbour, T. R.; Sakiyama-Elbert, S. E. The Effect of Endosomal Escape Peptides on in Vitro Gene Delivery of Polyethylene Glycol-Based Vehicles. *J. Gene Med.* **2008**, *10*, 1134–1149.